

Santa Clara University

Scholar Commons

Mechanical Engineering Senior Theses

Engineering Senior Theses

6-2022

Proof of Concept Mars Rover Crash Vehicle Test Article

Peter Habelt

Benjamin Rupp

Gavin Maloney

Stan Lieberman

Reid Whitney

Follow this and additional works at: https://scholarcommons.scu.edu/mech_senior



Part of the [Mechanical Engineering Commons](#)

SANTA CLARA UNIVERSITY
Department of Mechanical Engineering

I HEREBY RECOMMEND THAT THE THESIS PREPARED
UNDER MY SUPERVISION BY
Peter Habelt, Stan Lieberman, Benjamin Rupp, Gavin Maloney, Reid Whitney

ENTITLED
PROOF OF CONCEPT MARS ROVER CRASH VEHICLE TEST ARTICLE

BE ACCEPTED IN PARTIAL FULFILLMENT OF THE REQUIREMENTS
FOR THE DEGREE OF
BACHELOR OF SCIENCE
IN
MECHANICAL ENGINEERING



Thesis Advisor 6/9/2022
Date



Thesis Advisor 6/9/2022
Date



Department Chair 06/13/22
Date



PROOF OF CONCEPT MARS ROVER CRASH VEHICLE TEST ARTICLE

Senior Design Project Report

Submitted to

Department of Mechanical Engineering

of

SANTA CLARA UNIVERSITY

in Partial Fulfillment of the Degree Requirements for the degree of Bachelor of Science in
Mechanical Engineering

Santa Clara, California

2022

Proof of Concept Mars Rover Crash Vehicle Test Article

Peter Habelt, Benjamin Rupp, Gavin Maloney, Stan Lieberman, Reid Whitney

Department of Mechanical Engineering
Santa Clara University
2022

Abstract

The goal of the Mars Rover Crash Vehicle Test Article is to act as an impact-absorbing crumple-zone structure that protects a Mars Rover in the case of failure of other landing systems. This crash vehicle was designed for free-fall applications to absorb drops from different heights due to its modular crumple zone system. The design utilized readily available and recycled materials to create a low-cost, quick-build-time, modular system.

The design was split into two subsystems-the Crumple Zone and Inner Vessel-that would be placed inside and around the Outer Frame. The Crumple Zone underwent various iterations with the final design being columns of aluminum cans at the four corners of the Outer Frame. The Inner Vessel consisted of shock absorbers mounted to the sides of the Outer Frame that held the platform on which the Mars Rover would rest.

This scaled down design underwent three drop tests from a height of three meters. The first two tests utilized 144 aluminum cans for a maximum crumpling distance of 40.64 cm. These tests saw very little plastic deformation in the Crumple Zone and a 15 cm bounce after ground-impact, leading to the discovery of unwanted friction within the system. Additionally, the recorded acceleration data only gave a maximum acceleration of 6.28 g's when 30 were expected due to the accelerometers only recorded at a sampling rate of 14 Hz and not the expected 250 Hz. Because of these errors in these tests, the system and testing procedure were modified for a third test.

The third test saw the system mass increase by 22.6 kg, a Crumple Zone of 72 cans of 20.32 cm maximum crumpling distance, and a maximum sampling rate setting of 1250 Hz. Although only 52 Hz were achieved, the system behaved as expected, and recorded an acceleration of 21.02 g's, had no rebound, and absorbed 17.73J per can. The successes from this test indicate that scaling up this design is cost-effective and feasible for a Mars Rover with a mass upwards of 1000 kg.

Acknowledgments

We would like to express our deepest gratitude to our advisors Dr. Drazen Fabris and Dr. Nikola Djordjevic for their continued guidance, support, and patience throughout this project. The knowledge and expertise they shared demonstrated their care for their students and allowed for the insightful learning and exciting successes seen by this project.

Though not our advisors, this project would not have been possible without help from Dr. Calvin Tszeng and Rod Broome. The insight and guidance Dr. Tszeng provided in the design of our testing equipment allowed for successful, reliable, and safe drop tests. The machining and assembly of our project was greatly supported by Rod Broome, who was always eager to help and watch us succeed. From donating scrap material for us to implement, to teaching us new machining techniques, Rod's help played a critical role in the manufacturing of our project.

Table of Contents

| | Page |
|--|-------------|
| Abstract..... | iii |
| Acknowledgments..... | iv |
| Chapter 1: Introduction..... | 1 |
| 1.1 Introduction | 1 |
| 1.2 Motivation | 2 |
| 1.3 Background | 3 |
| 1.4 Goals and Objective | 3 |
| Chapter 2: Research and Conceptual Design..... | 5 |
| 2.1 Market Research | 5 |
| 2.2 Customer Needs & Product Specs | 7 |
| 2.3 Team & Project Management | 10 |
| 2.4 Design Process | 12 |
| Chapter 3: Final Subsystem Design and Analysis..... | 18 |
| 3.1 Baseline Testing | 18 |
| 3.2 Crumple Zone | 22 |
| 3.3 Outer Frame | 24 |
| 3.4 FEA Analysis | 24 |
| 3.5 Data Acquisition | 29 |
| Chapter 4: Manufacturing & Assembly..... | 30 |
| 4.1 Manufacturing Plan and Procurement | 30 |
| 4.2 Machining | 30 |
| 4.3 Assembly | 30 |
| 4.4 Test Assembly and Setup | 32 |
| Chapter 5: System Integration..... | 33 |
| 5.1 Ground Support Equipment [*] | 33 |

| | |
|--|-----------|
| 5.2 Safety and Procedure | 34 |
| Chapter 6: Test Results and Analysis..... | 36 |
| 6.1 Drop Test One and Two Results | 36 |
| 6.2 Drop Test One and Two Analysis | 39 |
| 6.3 Drop Test Three Results | 41 |
| 6.4 Drop Test Three Analysis | 43 |
| 6.5 Comparing Test Results to Goal | 45 |
| Chapter 7: Cost Analysis..... | 46 |
| 7.1 Bill of Materials | 46 |
| Chapter 8: Engineering Standards and Realistic Constraints..... | 48 |
| 8.1 Ethical Justification | 48 |
| 8.2 Environmental Impact & Sustainability | 48 |
| 8.3 Manufacturability | 48 |
| 8.4 Health and Safety | 49 |
| Chapter 9: Scaling Up the Design..... | 50 |
| Chapter 10: Summary and Conclusions..... | 51 |
| 10.1 Other Practical Use | 51 |
| 10.2 Lessons Learned | 51 |
| 10.3 Summary | 52 |
| References..... | 53 |
| Appendix A: Internal Concept Generation of Subsystems | 55 |
| Appendix B: Photos of External Designs | 57 |
| Appendix C: Photos of System | 58 |
| Appendix D: Timeline and Gantt Chart | 59 |
| Appendix E: Accelerometer Datasheet | 60 |
| Appendix F: Assembly Drawings | 61 |
| Appendix G: Copy of Conference Slideshow | 65 |

List of Figures

| | Page |
|---|-------------|
| <i>Figure 1.1: Preliminary system sketch.....</i> | 2 |
| <i>Figure 2.1: Images of the NASA Impact Spheres Key Components and Crumple Zone.....</i> | 5 |
| <i>Figure 2.2: Components of Different Energy Absorption Systems.....</i> | 6 |
| <i>Figure 2.3: Crumple Zone Aluminum Can Layout.....</i> | 12 |
| <i>Figure 2.4: Inner Vessel Shock Absorption.....</i> | 12 |
| <i>Figure 2.5: Multi-directional Shocks Kinematic Analysis.....</i> | 14 |
| <i>Figure 3.1: Initial Mockup Drop Test Fixture.....</i> | 18 |
| <i>Figure 3.2: CAD Model of Crumple Zone Subsystem.....</i> | 19 |
| <i>Figure 3.3: CAD Model of the Load Frame.....</i> | 19 |
| <i>Figure 3.4: CAD Model of Inner Vessel Subsystem.....</i> | 18 |
| <i>Figure 3.5: Crumple Zone Leg Assembly.....</i> | 21 |
| <i>Figure 3.6: Reinforced Frame Corners.....</i> | 22 |
| <i>Figure 3.7: Original and New System Design.....</i> | 23 |
| <i>Figure 3.8: Cross-Sectional View of Corner Mount Attaching to Beam.....</i> | 24 |
| <i>Figure 3.9: Shearing on Bolt.....</i> | 24 |
| <i>Figure 3.10: Shear in Bolt FEA with Exaggerated Deformation.....</i> | 26 |
| <i>Figure 3.11: Analysis of a Fixed-Ends Beam.....</i> | 27 |
| <i>Figure 3.12: Distributed Load, Fixed-Ends Beam.....</i> | 28 |
| <i>Figure 4.1: Assembled Base of Frame.....</i> | 30 |
| <i>Figure 4.2: Assembled Leg and Attached to Frame.....</i> | 30 |
| <i>Figure 5.1: Two-Dimensional Example of Cantilever Test Setup.....</i> | 32 |
| <i>Figure 5.2: Image of Actual Ground Support Equipment Setup.....</i> | 34 |
| <i>Figure 6.1: Live Image Taken Immediately Following Initial Impact of Test One.....</i> | 36 |
| <i>Figure 6.2: Test Article's State After First Two Drop Tests.....</i> | 37 |
| <i>Figure 6.3: Accelerometer Data from Drop Test One.....</i> | 38 |

| | |
|--|----|
| <i>Figure 6.4: Accelerometer Data from Drop Test Two.....</i> | 38 |
| <i>Figure 6.5: Accelerometer #1 Data from Drop Test Three.....</i> | 42 |
| <i>Figure 6.6: Accelerometer #2 Data from Drop Test Three.....</i> | 43 |
| <i>Figure 9.1: Artist’s Depiction of the Curiosity Rover’s “Sky Crane Maneuver”.....</i> | 50 |

List of Tables

| | Page |
|--|-------------|
| <i>Table 2.1: Design Specifications</i> | 8 |
| <i>Table 2.2: Testing Criteria</i> | 9 |
| <i>Table 2.3: Comparison of Externally Generated Designs</i> | 15 |
| <i>Table 2.4: Internal Design Sketches</i> | 16 |
| <i>Table 2.5: Design Selection Matrix</i> | 17 |
| <i>Table 7.1: Bill of Materials</i> | 48 |

Chapter 1: Introduction

1.1 Introduction

The goal of this project is to design, engineer, and fabricate a test article of a crash vehicle that protects a model Mars rover in the contingent case of partial failure in the parachute and thruster entry, descent, and landing systems. The idea for our design was initially based on a previous senior design project that involved a similar concept of a Mars Rover Crash Vehicle. That group had designed a similar device which used aluminum cans as a means of absorbing an impact [7]. We analyzed their design and decided to expand on their original design by testing different orientations of the cans that would allow us to maximize energy absorption. There will be three main subsystems to the crash vehicle: the Crumple Zone Subsystem, Inner Vessel Subsystem, and the Payload Hold Subsystem. These three subsystems will allow for a model Mars Rover to be secure in an impact that the crash vehicle absorbs. As a group, we decided to focus on testing different methods of impact absorption to find the best design for maximizing overall energy absorption during the crash. The first impact absorption subsystem would include an outer layer of hollow aluminum cans creating a crumple zone underneath the designated impact surface of the aluminum frame. The second system will be a system of shocks that are inside the frame that are designed to absorb any energy not absorbed by the aluminum can crumple zone.

The Payload Hold Subsystem is designed to keep the Mars Rover secure during the crash that the vehicle experiences. The main job of the other two subsystems is to absorb the impact but the Payload Hold is strictly designed to keep the Rover from rattling around and getting broken on impact. Different solutions were explored on how to secure the rover in the Payload Hold but the team decided on a six-sided connection system that will anchor the Rover in the Payload Hold from six points. This will allow the crash vehicle to crumple and absorb the energy of the crash while the rover stays in working condition.

The two aluminum frames will not need to be replaced after crashes so the only replacement a customer would have to make is in the aluminum cans that got crushed from the impact. Also, all the parts will be simple to replace if there come any issues to them. The importance of the project is to establish a cheaper and more efficient method of constructing and using/reusing a crash vehicle that has a very high success rate of keeping the payload, or rover, in good working condition. We are looking for a way to keep a Mars Rover safe to run more than

one mission on Mars. We believe that by engineering the project to be a sustainable and frugal option, that will allow for a greater impact on those who are involved.

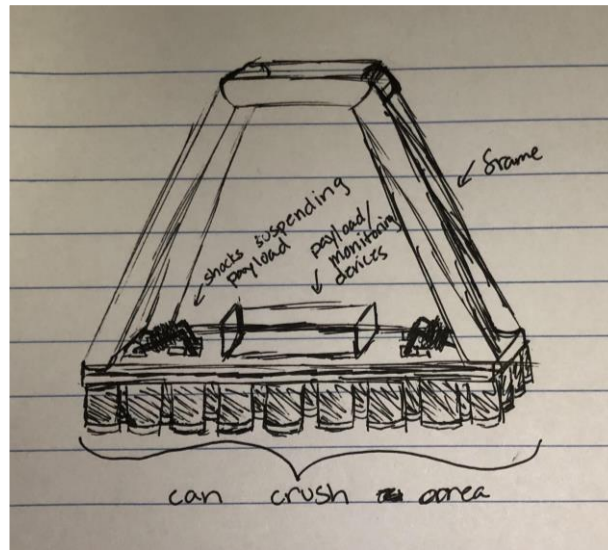


Figure 1.1: Preliminary system sketch

1.2 Motivation

Over the past decade, there has been a significant shift in the space industry as private corporations such as SpaceX, Blue Origin, and Virgin Galactic have joined, and in some ways even surpassed, NASA in pushing the frontier of off-planet exploration. Now that the space industry of the United States no longer solely consists of government-controlled NASA, there has been a huge acceleration in development of space systems and crafts, not to mention a large uptick in public interest in exploring beyond our world. As a nation, and even as a planet, we have never had such a sizable, capable, and well-equipped space industry, and the ambitions of these corporations reflect that.

Over the past decade, Virgin Galactic and Blue Origin have pioneered commercial spaceflight, while SpaceX drastically cut launch costs with the introduction of its reusable Falcon 9. Furthermore, Elon Musk the CEO of SpaceX, has projected that his company will send a manned mission to Mars in 2029, the 60th anniversary of the moon landing, and eventually initiate colonization efforts. As a result, it is predictable that the frequency of missions sent to the red planet will increase over the next few decades, which is a tremendous feat, especially in a financial sense. Therefore, we concluded that it would be beneficial to explore a means of lander contingency since a spacecraft must travel for approximately six months in the harshest environment known to man and execute its landing procedure properly upon reaching mars with no means of system maintenance or testing. Currently, in the event of any kind of landing failure,

even partial, the likelihood of vehicle destruction and mission failure is effectively guaranteed due to the brutal nature of planetary entry, but before any manned mission or further significant investment occurs, it would be beneficial to develop a partial lander failsafe to ensure the safety and security of any living or supply payloads sent to Mars and beyond.

1.3 Background

Previous Mars missions, all executed by NASA and federal space agencies of other nations, have seen the use of impact absorbing technologies as primary components of the various landers' landing sequences. Chief among these is the deployment of large airbags to surround the lander, as seen on NASA's Curiosity lander, and integrated shock absorbers as seen on Viking 1 & 2. Shock absorbers alone, however, are not capable of withstanding a significant impact and only serve to settle the rover in a stable manner once the landing thruster completes firing. After conducting research on existing and used landing solutions, we discovered that research into an absorption solution based on plastic deformation was extremely limited, except for a previous Santa Clara University Senior Design Project titled *Proof of Concept Planetary Lander Test Article* (2015), which exhibited the feasibility of a scaled down lander using plastic deformation as a partial impact absorption method.

1.4 Goals and Objectives

Our goal for this project was to design, engineer, and fabricate a small-scale planetary crash vehicle test article to study and uncover the feasibility of plastic deformation as a means for a contingency impact absorption method in a planetary landing scenario. Furthermore, we sought to explore the merits of arranging the cans in such a way as to increase the deformation distance compared to the design featured in the *Proof of Concept Planetary Lander Test Article*. We aimed to generate accelerometer data from test drops of the test article and analyze it to gauge the performance and feasibility of not only our design but also designed plastic deformation as an impact absorption method in our thesis. All these goals were accomplished.

Chapter 2: Research and Conceptual Design

2.1 Market Research

Through our research, we found various techniques which have been researched and previously designed to minimize impact loads. These shock alleviation techniques can be classified as hard landers (penetrators), semi-hard landers, and shock alleviators. Penetrators are designed to impact a surface with enough force to penetrate it and are slowed quickly by friction. Semi-hard landers utilize technologies such as airbags and crumple zones to slow the vehicle upon impact. Shock alleviators use dynamic systems often in the form of spring-dampeners, which are usually bulky and heavy, and the more widely used and preferred irreversible deformation devices, such as crushable infills and foams.

NASA published an article in which they discuss the design of a sample EEV, or Earth Entry Vehicle, that could be used in a Mars Return Mission. The design of the EEV consists of an outer shell of hexagonal shells made from Kevlar and filled with composite foam. These cells act as the crumple zone that absorbs the energy at impact when the sphere hits the Earth. Additionally, there is an Accelerometer in the Payload Hold, the inner compartment where the rover will be held, that provides data for acceleration, velocity, and deformation results [2]. This design is very similar to the design we were wanting to create for the crash vehicle. The crumple zone feature will be one of the main subsystems and we can apply the hexagonal cell design into the design as well.

The design of these impact spheres shared many similarities to the design which we initially had for the design of the system. The first of these commonalities was the cellular structure built around the sphere. Using hollow cells to crush and absorb energy is what we planned on doing for the design. However, the Kevlar and carbon foam-filled cells were not feasible due to the cost. Instead, we decided to use empty aluminum cans to provide the same purpose as the cells. These cans are much cheaper and more sustainable than the Kevlar cells. Secondly, the NASA spheres use accelerometers which are centrally located inside the sphere to take measurements during the testing of the sphere. With these accelerometers, we would be able to take necessary measurements, like acceleration and shock, to understand how much energy the system is absorbing.

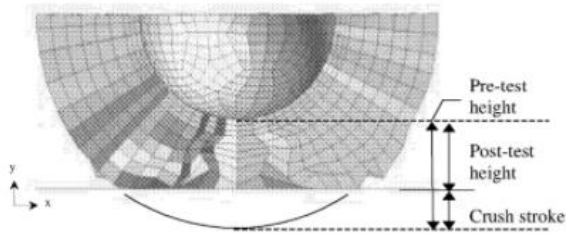


Figure 18 – Cross-section of deformed cellular structure #1, $t = 0.002$ s.

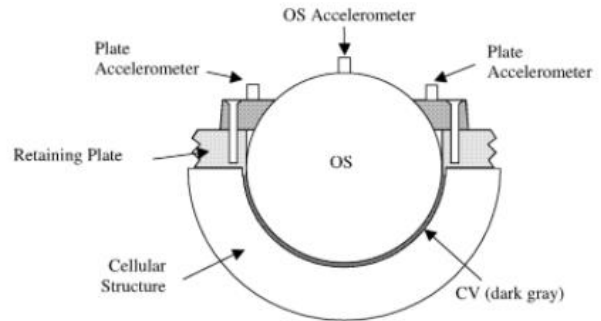
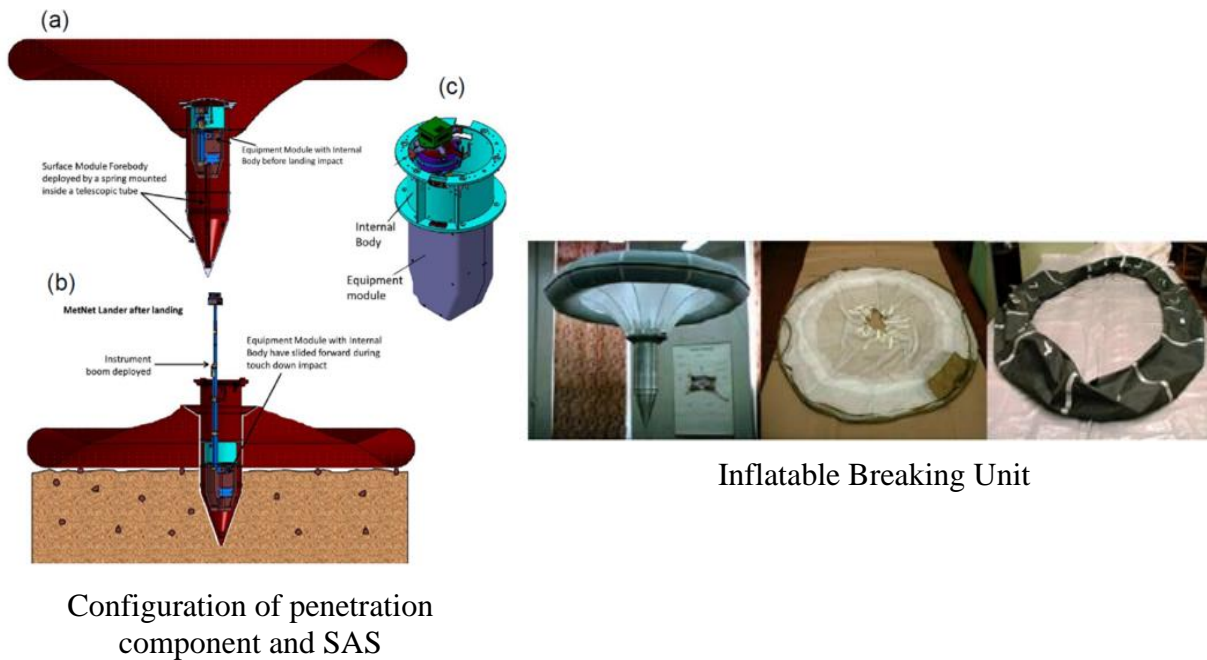


Figure 4 – Typical impact test specimen for test #4.

Figure 2.1: Images of the NASA Impact Spheres key components and crumple zone via: Billings, Marcus. NASA Impact Spheres (reproduced without permission).

Another system that was found useful for understanding the capabilities of the project was involving MNL and its various shock alleviation systems. This design was useful because it utilizes many different techniques in different stages of the impact landing. The system consists of penetration landing, inflatable structures, deforming components, and dynamic shock absorption. This provides a good example of how to combine different tools to form a superior vehicle, versus simply using one technique that can be adequate. This particular design is intended to deliver meteorological instruments to Mars, but the ideas here can be utilized and expanded upon to fit the use case for a rover [6]. We found many opportunities for improving this system and adapting it to the needs by replacing the inflatable system with a crumple zone or metal foams to provide greater security for a rover, which would likely have a greater mass than the instruments depicted in the study. As far as the implementation of these systems were concerned, the airbags were the only shock-alleviating system that we felt we could continue further discussion on. The other systems, like the penetrating body, would have caused too much damage to the on-campus testing facilities we were to use. We felt that this system was most useful because it described a variety of different impact-absorbing systems that worked together. As a group, we knew that we would have to consider multiple methods of energy absorption due to the resources we would have access to.



*Figure 2.2: Components of Different Energy Absorption Systems
via: ExoMars 2022 (reproduced without permission)*

2.2 Customer Needs & Product Specifications

NASA cites that only 40% of the missions ever sent to Mars, by any space agency, have been successful [1]. Landing the mission vehicle safely and successfully on the surface of the planet is the most crucial step in having these missions succeed. Therefore, having a robust and reliable landing system is a critical aspect of every mission to Mars. For the project, focusing on Mars Rover crash vehicle systems, the customer base anticipated for this project is primarily NASA. Up until this point, NASA has been the most predominant party involved in subsidizing, planning, and executing exploration missions to the planet Mars that rely heavily on the safety and reliability of entry, descent, and landing systems such as those that are the focus of this project. We understand it is possible that newer, private aerospace companies such as SpaceX, would be other potential customers for a product such as this. However, it is also the case that any company or organization with the intention of launching and landing a successful mission to Mars, could be a potential customer to the technologies we wish to investigate in the scope of the project.

Following the deployment of several parachutes to slow descent to manageable speeds, previous Mars Rover landing systems have utilized deployable airbag systems to safely land the vehicle from the final stage of descent to the Martian surface. The airbag systems were responsible

for absorbing the impact of the vehicle after hitting the hard and rocky surface of Mars at up to 20 meters per second. The airbags were arranged in a lattice structure of 24 spherical bags resembling a bundle of grapes that surrounded the Mars Rover vehicle, and were made from an extremely durable, synthetic fabric called Velcran, which is also used to make spacesuits. This method was utilized for the Pathfinder and Mars Exploration Rover missions. Due to the increased payload mass of the Mars Exploration Rover mission, the airbag landing system went through a redesign that implemented a double-bladder airbag design. The greatest advantage that this final stage landing system brought to the Mars Rover missions was significant mass savings, which allowed NASA to include the microrover, Southerner, on its Pathfinder mission.

On more recent Mars Rover missions, the vehicles containing Rovers have been increasingly larger in mass. Another prominent final stage landing system utilized for NASA Mars Rover missions was rocket assisted descent. Parachutes equipped in conjunction with these systems only slow the vehicle to a velocity of 89 meters per second, where at this stage they detach from the payload and give the responsibility of safely delivering the payload to the surface of Mars to the final stage rocket thrusters, which slow the vehicle to a safe landing velocity. This system uses a set of the downward and laterally facing rocket thrusters to reduce the vehicle's velocity to under 6 meters per second so that it could land safely without damaging any of the critical mission components. In the most recent NASA Mars Rover missions such as Curiosity and Perseverance, rocket-assisted descent has been used in conjunction with a sky crane that has lowered the Mars Rover vehicle from an altitude of 21 meters at a constant velocity of 0.75 meters per second [10].

Without the use of rocket assisted descent thrusters, there would be only a small chance that any impact absorbing system such as an airbag configuration or crumple zone would be capable of safely landing the Mars Rover from speeds greater than 89 meters per second. Therefore, we focused the work on developing a system that would emulate a system responsible for safely landing and protecting the payload in case of failure of the very final stage of landing, such as a failure of rocket-assisted descent thrusters or other systems previously discussed. A goal velocity to safely absorb the landing impact from would be in the range of 13-45 meters per second, with 13 meters per second being the minimum viable velocity for the system to successfully protect the payload from a crash landing.

For the project, we initially planned to drop a 45 kg load from a given height and test three different crash vehicles that will protect the load from any visible plastic deformation, stress, and shock fractures. Considering this project being the next step from the 2015 Planetary Lander

Concept project, we used their target specifications for the desired energy absorption, mass, volume, and drop height. Although these values were slightly altered as the project develops through modifications and feasibility assessments, below are the preliminary metrics we would like to achieve. Some metrics were translated and scaled down from the Mars Rover Opportunity landing and others were from the own desired goals. The metric ranks were determined in order of both subjective and objective customer/team needs.

Table 2.1 Design Specifications

| Metric Rank | Metric | Numerical Value | Units |
|--------------------|---|------------------------|---------------------|
| 1 | minimum energy absorption | 5141.6 | J |
| 2 | mass of lander | < 45 | kg |
| 3 | mass of rover vehicle (payload) | 20.4 | kg |
| 4 | total volume of lander | < 1 | m^3 |
| 4 | max aerodynamic roll/pitch (from tdc*) | 5 | ϕ (degrees) |

*tdc = top dead center (is 0 degrees, the noon position on a clock)

Beyond NASA and the multitude of private astronomical corporations, we also considered using military air drops as another reference for the energy absorption strategy. For example, in order to deliver equipment and vehicles to isolated areas and units, the military will secure a Humvee to a metal platform with the necessary supplies and parachutes attached. These platforms are then jettisoned above the drop location where three parachutes deploy to slow the immense payload's descent. Upon reaching the ground, a crushable honeycomb structure beneath the vehicle as well as the full travel of the vehicle's suspension cushion the impact. This enables the payload to impact the ground at a maximum of 9 meters per second upon which the Humvee's suspension will be fully compressed. Even though these airdrops occur in Earth's atmosphere, we can extrapolate parachute, mass, and even impact absorption numbers and systems to a Martian environment to better refine the methods for impact absorption for the Martian Crash Lander and apply existing solutions to new scenarios.

Table 2.2 Testing Criteria

| Metric Rank | Metric | Numerical Value | Units |
|--------------------|--------------------------------|------------------------|----------------|
| 1 | Desired Drop Height | 10 | m |
| 2 | Desired Drop Terminal Velocity | 13.86 | m/s |
| 3 | Target area size | 2 | m ² |
| 4 | Desired Landing Orientation | 0 ± 5 | Φ degrees |

Along with desired product specifications of the crash vehicle, we also designated specific testing criteria the vehicle should meet during the testing of the system. We initially planned on dropping the crash vehicle from 10 meters. This height was chosen because it will allow us to reach the desired terminal velocity of the crash vehicle. If this terminal velocity is achieved, we will get more accurate measurements that are comparable to those of a Mars Rover vehicle that will crash land on the surface of Mars. The target landing area of the crash vehicle will be 2 square meters. The small size of the landing area will ensure a more accurate drop that eliminates an offset from the zero degrees for the desired landing orientation.

2.3 Team & Project Management

Project Challenges & Constraints

The project's challenges revolved around the mission goal that a load in free fall would need to remain in the same condition it was packaged in upon landing. These challenges included lowering impulse, distributing localized shock, landing upright, maximizing kinetic energy redistribution via the beverage cans, and keeping the weight and vehicle packaging size at a minimum. The project constraints that dictated the design process were the maximum acceleration, weight, and cost. Additionally, constraints that influenced the design were safety, manufacturability, and use of readily and widely available off-the-shelf parts.

Design Process

The team began the project by identifying the potential and actual stakeholders of the mission, researching existing solutions, and then formulating a plan of action for how to approach building a ground-up design. The plan was guided by the idea of improving the previous *Proof of Concept Planetary Lander Test Article* (2015) and tweaking the mission requirements to what

would work better with the Perseverance Rover's Entry, Descent, and Landing Vehicle as opposed to the Spirit Rover.

The team used the guide project's laboratory research on aluminum can buckling energy requirements and paired it with self-made preliminary empirical drop tests identifying aluminum can buckling energy. Then sketches and design matrices were brainstormed and discussed, which led to the final design configuration seen in the CDR. The design was built and tested, where new problems were identified, fixed, and tested again to aim for clearer data and performance results in the iterative engineering process.

Timeline

The project timeline was scheduled via Gantt charts and utilized the method of creating smaller deliverables from bigger project goals/milestones. Reaching smaller deliverables allowed the team to increase efficiency. The team could check in more often on progress, identify problems earlier on, and adjust the schedule accordingly. This strategy allowed for more flexibility when reorganizing and reprioritizing as deliverables were being finished.

Budgetary Constraints

The provided budget was \$2457, and a large portion was allocated to procuring 3 wireless accelerometers and the Ground Support & Test Equipment. The Bill of Materials includes the breakdown of parts and cost, and it has the three main sections of the project materials: frame parts, testing equipment, and accelerometers. The cans, rope, and acrylic plates were acquired through personal means and did not affect the budget. A closer look at the Bill of Materials for the entire project can be found on *Table 7.1*.

Team Management

The team operated as what people in research and development might be familiar with. The team worked in sub-groups of 2 or 3 people with tasks that were self-assigned or delegated by the team-nominated manager. Using a combination of group messaging and face-to-face meetings, the group communicated effectively and efficiently to identify what work needed to be done and by when.

Risks

The project assumed most risks in the testing portion. Dropping from a height above 2m required locating and reserving a location on campus that had low foot-traffic, a second story balcony, and an open and flat ground floor. Campus Safety allocated a space in the parking lot of 733 Benton St. after a proposal showing the safety calculations and OSHA requirements for balcony railing strength, of which was needed to support the cantilever test beam. During testing, the team used dumpsters and 4'x8' (1/4" thick) plywood sheets for shrapnel protection. Safety glasses were worn, only one person would announce the drop countdown, and people remained at a self-determined safe distance away from the drop. The testing was supervised by our thesis advisor and machine shop manager.

2.4 Design Process

The system was constructed of three subsystems. The Crumple Zone acted as the first and primary source of impact absorption. This would likely be a one-time-use system and designed to a degree in which the system would not bounce off the ground after impact. The Inner Vessel consists of a second source of energy absorption that serves to absorb the energy not absorbed by the Crumple Zone. The Inner Vessel would likely take the form of an arrangement of shock absorbers on pivots so it could also settle the payload's momentum if there is rotation in the system.

Crumple Zone Subsystem

The Crumple Zone Subsystem is acting as the first line of defense when it comes to impact absorption in the design. The crumple zone is meant to absorb an impact of the crash vehicle by "giving" when the vehicle impacts the ground. This means that we plan on the crumple zone being destroyed after each single testing phase. For example, if we were to use aluminum cans along the bottom of the vehicle to act as the crumple zone, they would all be crushed, given that the test runs correctly, and we would have to replace them before the next test. The crumple zone is meant to be the initial impact absorber of the crash vehicle so that the internal shocks do not have to do all the energy absorbing work.

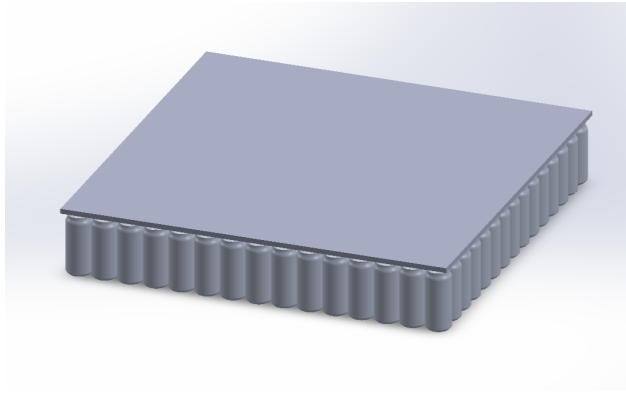


Figure 2.3: Crumple Zone Aluminum Can Layout

Inner Vessel Subsystem

The Inner Vessel Subsystem is designed as the second line of defense for the impact absorption of the design. Along with the Crumple Zone, the Inner Vessel will absorb the energy on felt impact when the crash vehicle hits the ground. We are planning on the Inner Vessel absorbing all the resulting energy that is not absorbed by the Crumple Zone. We plan on engineering this subsystem to connect the Payload Hold to the frame of the vehicle. The shocks will suspend the Payload Hold, allowing the Rover to have room to move freely within the inside of the frame without any damage being inflicted on it. The key part of the design criteria for this subsystem is the ability to keep the Payload Hold secure and in place while the shocks absorb whatever energy is still moving through the Crash Vehicle after the Crumple Zone Subsystem has played its role in energy absorption.

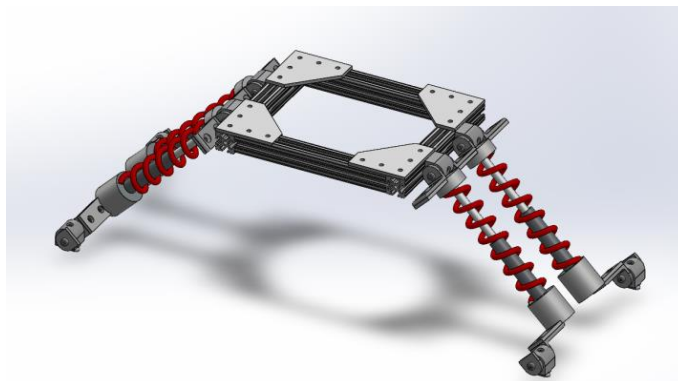


Figure 2.4: Inner Vessel Shock Absorption

Critical Design Criteria

The key design criteria are as follows:

1. Keep system size and mass to a minimum: it is critical that the crash lander vehicle's mass and volume be kept as small as possible which would allow the system to operate with full

functionality so that the crash lander vehicle does not substantially increase the total payload mass of the Mars Rover mission that it is operating in. Due to the critical significance of weight and space savings in these kinds of aerospace applications, structural strength components of the crash vehicle will be designed with an intended yield safety factor of close to 1.3 times the maximum loading conditions that the system will experience during operation.

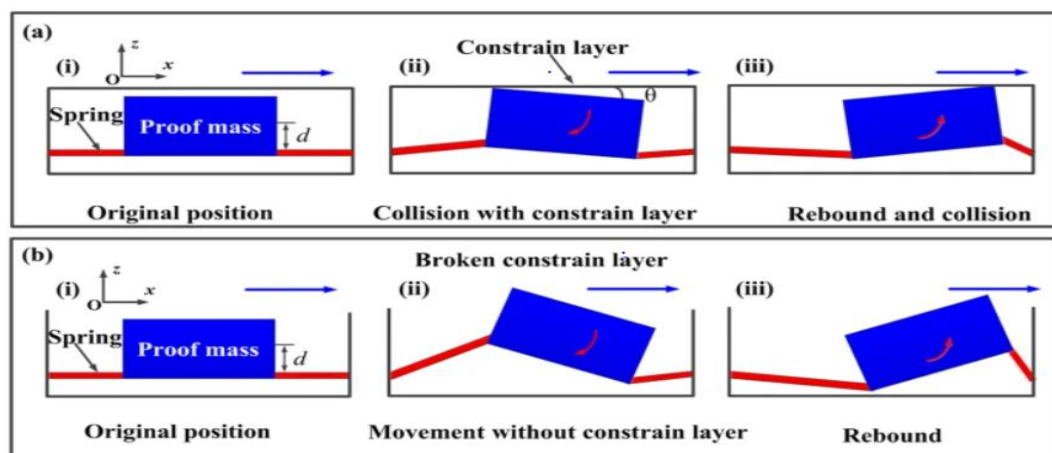
2. The system will be designed to safely land and absorb the impact of a small-scale Mars Rover vehicle such as the NASA Spirit and Opportunity rovers that landed on the surface of Mars in 2004. These rovers had an approximate weight of 250 kilograms. A full-scale model of the landing vehicle would be out of the scope of this project; therefore we will design the system to be able to safely land a model rover that is scaled to 10% of the NASA Spirit and Opportunity rover's weight (25 kg).
3. The amount of energy required to be dissipated by the NASA Opportunity Mars rover air bag systems upon landing was approximately 52 kJ. Therefore, we will design the system to absorb at least 5.2 kJ of energy upon impact.
4. The entire crash vehicle system will have an approximate volume of less than 1 cubic meter and total system mass of less than 45 kg.
5. The system will be drop tested from heights of 3, 6, and 10 meters to verify the effectiveness of the design.

External Concept Design Search

As a team, we did research on several different previously existing systems that incorporate impact absorption. We analyzed the scope of the systems and broke down what we believed would be the most helpful for us.

- NASA Energy Absorption Impact Sphere
 - NASA has created a design for a sphere that absorbs an impact using foam-filled cells surrounding the outside that work as a crumple zone for the sphere. This is similar to the idea of the crumple zone at the bottom of the crash vehicle. Like us, the impact sphere has accelerometers to calculate the required energy absorbing power of the crumple zone. However, the geometry of this sphere does not fit the design criteria for the vehicle. We plan to test the impact absorption systems by dropping the vehicle vertically and so we are putting an importance on a flat base of the crash vehicle rather than a rounded one as shown by the NASA model [9].

- Inertial Microswitch with Multi-Directional Shocks
 - This design illustrates a system of multiple shocks that absorb an impact for specific payload. In this example, a small microswitch, which is the payload in this case, is attached to the circuit board with the struts. These struts are attached to the corners of the microswitch, and they suspend the payload above a hole in the circuit board. These struts are similar to what we were planning on working with for the Inner Vessel Subsystem. Like the microswitch struts, we want to design the shocks to suspend the payload hold from each of the corners. The struts will allow for the payload hold to be kept safe throughout the crash [12].



Rotation and movement process of the proof mass in moving toward stationary electrode (a) with constraint layer and (b) without constraint layer.

Figure 2.5: Multi-directional Shocks Kinematic Analysis via: "Microswitch Shock Resistibility" (reproduced without permission)

Concept Generation

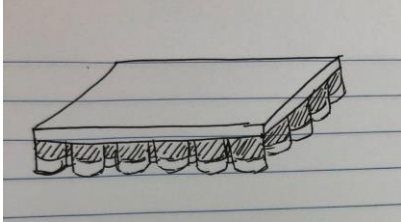
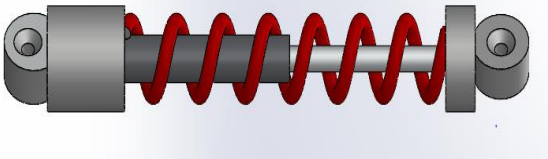
All the internally and externally generated designs for each subsystem were laid out and their pros and cons were assessed and compared. The following tables include benefits and drawbacks of each design and a selection matrix where final configurations were chosen. *Table 2.3* shows the drawbacks and benefits of each previously existing design we researched. This was helpful to highlight the different pieces of each design we believed would be useful moving forward with our project.

Table 2.3: Comparison of Externally Generated Designs

| External Designs | Benefits | Drawbacks |
|---|--|---|
| NASA Impact Sphere (<i>Crumple Zone</i>) | <ul style="list-style-type: none"> ● Hollow cells crumple effectively from any direction ● Allows for greater margin of error | <ul style="list-style-type: none"> ● Circular base/poor geometry ● Difficult to manufacture ● High priced materials |
| Multi-Directional Shocks for Microswitch (<i>Inner Vessel</i>) | <ul style="list-style-type: none"> ● Uses struts with more than one axis of motion ● Shares geometry with the previous shocks design ● Designed to be anchored to the corners of a rectangular device | <ul style="list-style-type: none"> ● Struts work better with a constraint layer ● Difficult to scale ● Microswitch is not completely suspended |

Below, in *Table 2.4*, we illustrated the sketches generated by our team for different subsystem ideas. Each subsystem had several sketches (shown in Appendix C), and we picked the top idea for each subsystem to move forward with.

Table 2.4: Internal Design Sketches

| Crumple Zone Subsystem | |
|---|---|
|  | <p>Aluminum Cans</p> <p>Aluminum cans serve as a scaled-down crumple zone that will permanently deform to allow the vehicle to decelerate. This method is lightweight and cheap but requires replacing cans after every test.</p> |
| Inner Vessel Subsystem | |
|  | <p>Linkage Shocks</p> <p>A platform with shock absorbers at each corner attached to the walls of the Inner Vessel. The linkage system ensures the platform and payload stay in an orthogonal plane during impact as well as ensuring security in a single plane of motion.</p> |

Selection

Each proposed subsystem design concept was scored based upon their ability to satisfy the critical design criteria to achieve the overall project goals. After careful discussion, examination, and consideration of each of the proposed subsystem design concepts and their design concept scores, a best design for each subsystem was chosen.

Table 2.5: Design Selection Matrix

| | Weighting (1-3) | 2 | 1 | 3 | 3 | 2 | Out of 70 |
|--------------|--------------------|-------------|-------------|-----------------|------------------|----------------|-------------|
| Sub-systems | Design Concept | System Mass | System Size | System Strength | Energy Absorbing | Cost of Design | Total Score |
| Inner Vessel | Microswitch Shocks | 4 | 5 | 2 | 2 | 4 | 45 |
| | Foam Barrier | 5 | 1 | 1 | 1 | 5 | 42 |
| | 8 Corner Shocks | 2 | 1 | 5 | 5 | 1 | 46 |
| | Linkage Shocks | 5 | 5 | 2 | 2 | 5 | 52 |
| Crumple Zone | NASA Impact Sphere | 3 | 3 | 4 | 5 | 1 | 41 |
| | Air Bag | 5 | 5 | 3 | 4 | 2 | 41 |
| | Cell Structure | 2 | 3 | 5 | 5 | 1 | 42 |
| | Aluminum Cans | 5 | 2 | 3 | 2 | 5 | 52 |

Regarding the Inner Vessel subsystem, the linkage shocks and platform layout was ranked the highest, the product champion, and intuitive in respect to the other concepts. It is lightweight, the least expensive, and simple to manufacture--all while maintaining its requirement for absorbing enough energy to protect the rover from mild impact and vibrations.

For the Crumple Zone subsystem, the aluminum can design ranked the highest of the proposed crumple zone options. Although this design did not score as well as the other options in robustness and absorption capabilities, it scored much higher in ease of manufacturing, cost, and

mass minimization. Since crumple zones are destroyed and must be rebuilt after each test, scoring well in these areas facilitates prototyping, testing, and iterative design.

Chapter 3: Final System-Level Design and Analysis

3.1 Baseline Testing

After the final designs were selected for each subsystem, we began creating CAD models of all the essential components of the subsystems. Beginning with the crumple zone subsystem, a lattice of aluminum cans was arranged beneath a flat base plate. To determine the appropriate number of aluminum cans required to absorb 5.2 kJ of kinetic energy, we first had to determine how much energy each can could absorb when crushed. Crumple testing using a universal testing machine performed by the previous senior design crash lander project estimated the energy absorbed by crumpling one can to be 97 J. To verify this result, we established a testing procedure of dropping a 20 kg mass from a height of 2 meters. Upon impact with the ground, the collision would result in approximately 400 J of energy needed to be dissipated for the mass to come to a complete stop. To verify the 97 J per can absorption metric, the cans were installed on the underside of the 20 kg mass.



Figure 3.1: Initial mockup drop test fixture

Following the drop test, it was concluded that the cans were insufficient in absorbing the total kinetic energy of the impact of the mass, as all the cans became completely crushed followed by the mass bouncing off the ground. The number of cans installed on the mass plate was then increased and the test was subsequently repeated until no recoil of the mass off the ground was observed following impact. After several repeated tests, the number of cans determined to be sufficient in completely absorbing the impact of the mass was 8. Therefore, it was concluded that each aluminum can absorbed approximately 47 J of energy due to crumpling, which was 50% less

than calculated by the previous senior design group. Following this conclusion, it was determined that there must be a significant correlation between the impact velocity and the energy absorbed per can. Assuming a linear correlation between the impact velocity and energy absorption per crumpled can, and extrapolating to a drop height of 10 meters, the expected energy to be absorbed per can is 23 J. Under this assumption, we can then determine the appropriate number of cans to absorb 5.2 kJ of kinetic energy to be approximately 225, which necessitates a 15x15 matrix of aluminum cans to constitute the crumple zone subsystem, as depicted in the CAD model shown below.

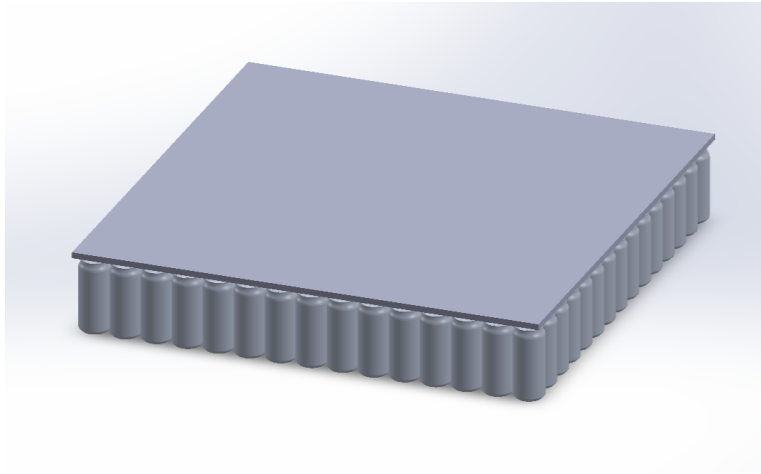


Figure 3.2: CAD Model of Crumple Zone Subsystem

The load frame was then designed to serve as a rigid support frame that both transfers the momentum forces from the crumple zone to the inner vessel and also protects the payload from being damaged due to any unexpected system failures. 80/20 Aluminum T-slotted framing rails were used due to their relative cost effectiveness, strength, and extreme utility and ease of manufacturing.

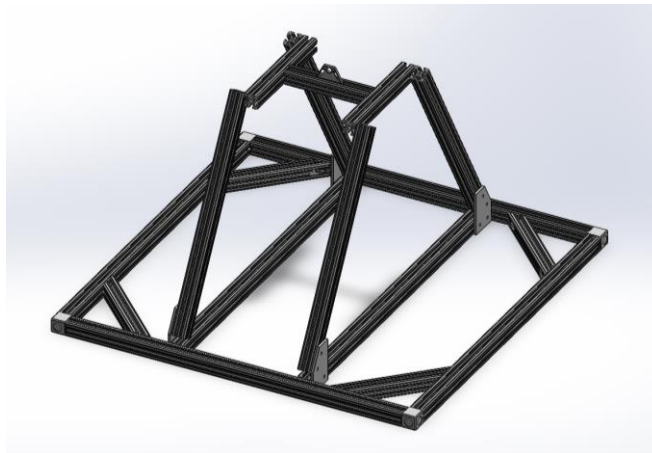


Figure 3.3: CAD Model of the Load Frame

The inner vessel subsystem consists of the shock absorbers on opposite sides of the rover. The shock absorbers are attached directly to the outer edges of the load frame on one end, and their other end is attached to the edges of the platform on which the rover rests. Both ends are on pivot mounts to allow fluid motion. The design consists of having the shock absorbers in pairs on only two sides of the platform to increase their strength. Although this eliminates most flexibility in the horizontal direction, this was deemed an acceptable trade-off because of the desired characteristics achieved by the rest of the system. The product specifications and testing criteria for the entire system require it to have a maximum aerodynamic roll of 5° and a horizontal landing orientation $\pm 5^\circ$. Assuming these values are met, there will be minimal forces acting on the horizontal plane and having the shock absorbers acting in the vertical direction will be adequate.

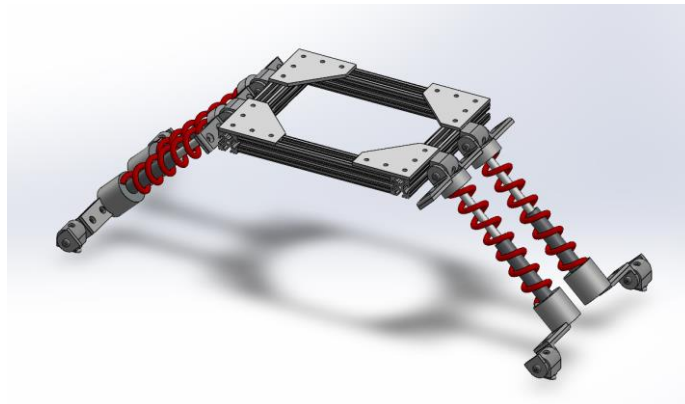


Figure 3.4: CAD Model of Inner Vessel Subsystem

3.2 Crumple Zone

An expected impact velocity of 14 m/s from a drop of 10 meters coincides with the impact velocity of the NASA Spirit and Opportunity rovers when landing on the surface of Mars as well as the values recorded during testing of the rover's airbag impact absorption system which we are intending on replacing with the crumple zone subsystem [1]. Furthermore, from this test report of the rover airbag landing systems, it was shown that the maximum acceleration that was experienced during simulation of the crash landing system was 26.4 g's. Therefore, we are designing the rover crash lander test article with a maximum acceleration of 30 g's (294.3 m/s^2) in mind. Using this value and an expected total system mass of approximately 50 kg, we can use a simple application of Newton's second law to determine that the maximum force due to acceleration that the total system will experience to be $F_{max} = 14.7 \text{ kN}$.

Relating work done to total potential energy removed from the system during impact, shown in Equation (1), brings an expected value of average force applied to the frame from the crumple zone subsystem of $F_{avg} = 51.18 \text{ kN}$.

$$F = \frac{K_e}{d} = \frac{5.2 \text{ kJ}}{10.16 \text{ cm}} = 51.18 \text{ kN} \quad (1)$$

The flaw in the original crumple zone subsystem that led to this much higher value of loading and average acceleration of over 1000 g's on the system was the extremely limited travel of suspension of the crumple zone. Therefore, the crumple zone subsystem was modified to have a much greater travel, and therefore allow for a lower loading over a greater distance and greatly decreased acceleration on the system.

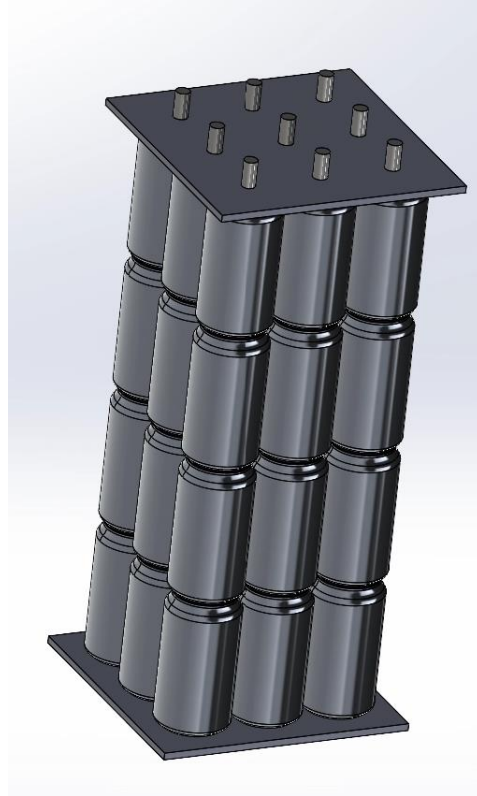


Figure 3.5: Crumple Zone Leg Assembly

The new iteration of the crumple zone subsystem utilizes 36 total cans in a 3x3x4 configuration. The increased travel of the new crumple zone lowers average load on the total system during compression. These cans will be fixed between aluminum plates on each end for normalized compression of each leg and guided by freely sliding aluminum rods that pass through the center of each can to maintain their axial positioning during deformation. Another advantage of

the new design iteration of the subsystem is that splitting the crumple zone system into the independent legs allows the system to better cope with system tilt upon landing.

The new design effectively raises the suspension travel to a maximum of 0.5 m. Reapplying the simple work formula, the value of average force that the crumple zone subsystem must exert to properly decelerate the system to a stop over 0.5 m of travel is 9.8 kN, which leads to a value of 272 N per can. The average acceleration that the system will experience during this event will be 20 g's. Now applying the work formula to each individual can in the crumple zone assembly, the work done by each individual can to decelerate the system to a stop will be $272 \text{ N} \cdot 0.122 \text{ m} = 33.2 \text{ J}$, which is less than the currently tested energy absorption per can of 47 J by a safety factor of 1.4.

3.3 Outer Frame

To accommodate for the new crumple columns, the outer frame was modified to have more robust corners. Since the crumple columns would need to be supported more than the original crumple layer spanning the entire bottom surface, the corners of the frame were reinforced to comfortably hold the top plates of the crumple columns.

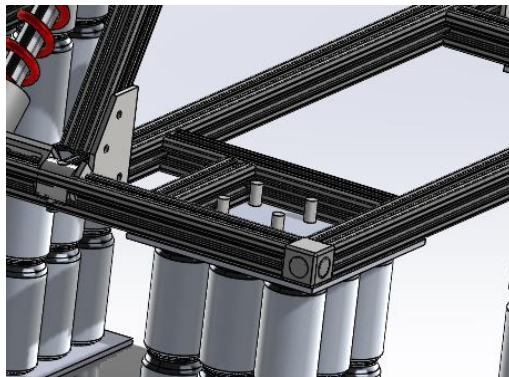


Figure 3.6: Reinforced Frame Corners

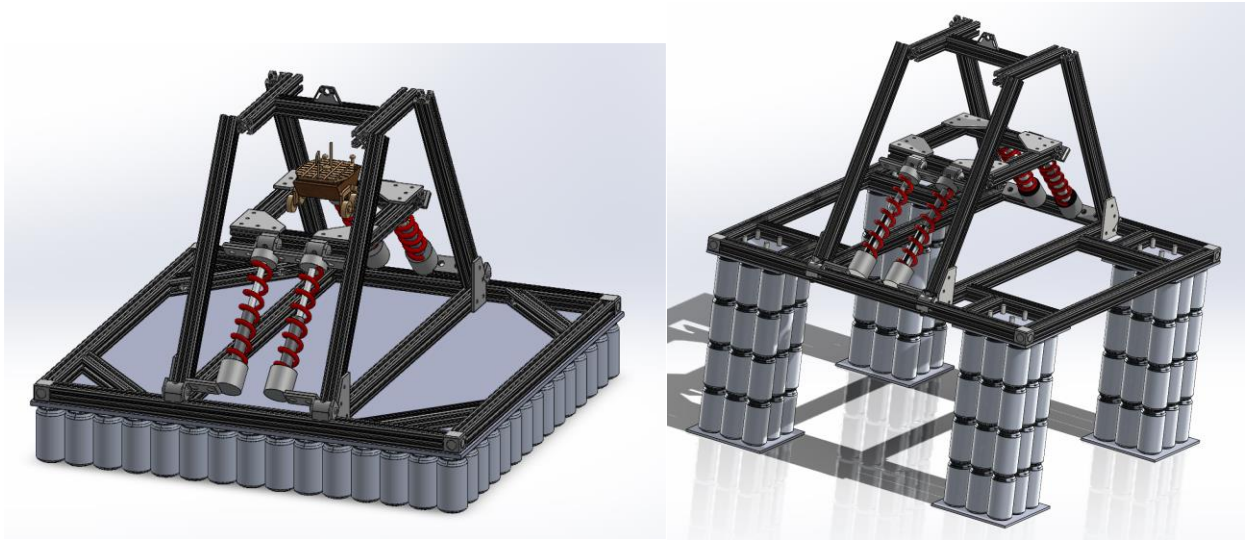


Fig. 3.7 Original (left) and New (right) System Design

3.4 FEA Analysis:

The test article as a structure features multiple individual and comprehensive parts and assemblies that can be analyzed for failure and deflection under static and dynamic conditions. The static shear stress on the corner joints (mounts) and static bending stress and deflection for a distributed load on a fixed-ends 80/20 beam were analyzed.

Impact Force

To perform calculations and simulations of the system under load, the impact force was calculated. Knowing 5.2 kJ will be needed to be dissipated for a safe landing, and the current crumple zone would crumple 10.16 cm (4 in), an average impact force of 51.18 kN was calculated, as shown below.

$$F = \frac{K_e}{d} = \frac{5.2 \text{ kJ}}{10.16 \text{ cm}} = 51.18 \text{ kN} \quad (2)$$

Corner Mounts

The corner mounts connecting the beams in the outer frame were chosen to be analyzed because regardless of whether the beams themselves would fail during operation, the components holding them together would need to be strong enough to withstand testing as well. The corner mount chosen uses a single bolt to connect the mount to the end of each beam, as shown below. Since the bolts are the only fastener, they receive the entire vertical load upon impact. Their bolts and the shearing stress they undergo were analyzed to determine if they would fail.

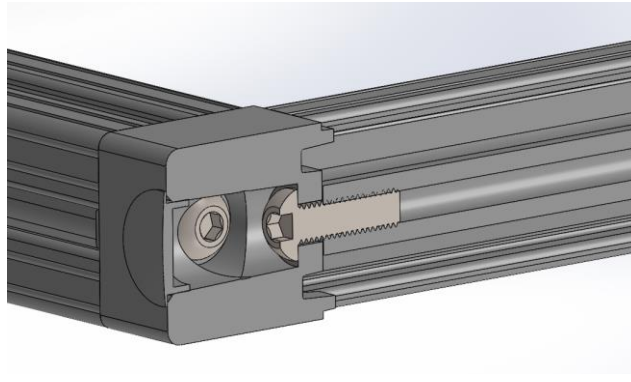


Figure 3.8: Cross-Sectional View of Corner Mount Attaching to Beam

Corner Mounts Analysis

The 51.18 kN impact force was distributed between the eight bolts found in the corners of the outer frame base, for 6.4 kN per bolt. The expected 6.4 kN was used as the impact force in the following bolt calculations.

The bolts analyzed were the 5/16x1 in SAE Grade 2 steel bolts that are included with the purchase of the selected corner mounts. With the bolt as the reference point, it is expected that the beam will move upward with force F , creating a shearing stress. A depiction of the shearing is shown in *Figure 3.10*.

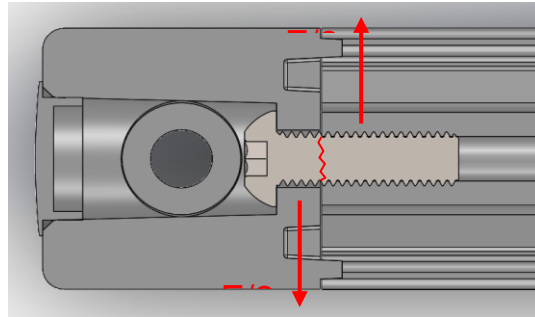


Figure 3.9: Shearing on Bolt

The shear in the bolt was calculated to be 135.14 MPa, as shown below.

$$A_c = \frac{\pi(5/16)^2}{4} = 0.0767 \text{ in}^2 = 0.049 \text{ cm}^2 \quad (3)$$

$$\tau = \frac{F}{A_c} = \frac{6.4 \text{ kN}}{0.49 \text{ cm}^2} = 135 \text{ MPa} \quad (4)$$

$$\sigma_y = 400 \text{ MPa} \quad (5)$$

$$n = \frac{400 \text{ MPa}}{135 \text{ MPa}} = 2.96 \quad (6)$$

Using the bolt's minimum yield strength of 399.91 MPa, a factor of safety of 2.96 was calculated. This is a very favorable result because it shows the bolt will not fail under the expected loading conditions and can take a larger load if necessary.

To confirm the calculated results, a finite element analysis was run on the bolt. Due to the dimensions of the corner bracket, shearing is expected 6 mm down the length of the bolt. The loading scenario was simulated by fixing the head of the bolt, applying a rotation restraint on the end of the bolt since no rotation is expected, and applying a downward force on one side of the analyzed plane, and an upward force on the other side to simulate shearing. *Figure 3.11* shows the simulation results with an exaggerated deformation for visual aid.

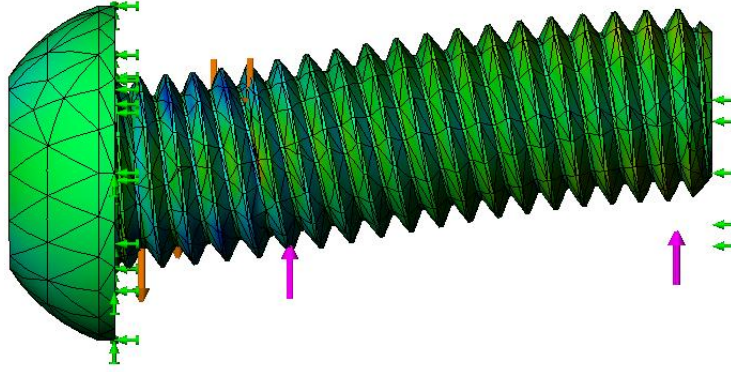


Figure 3.10: Shear in Bolt FEA with Exaggerated Deformation

The simulation showed a max shear of 22.62 kpsi in the desired cross-section. This value results in a factor of safety of 2.56, which is satisfactory and there would be no need to select stronger bolts.

$$\sigma_y = 400 \text{ MPa} \quad (7)$$

$$n = \frac{400 \text{ MPa}}{156 \text{ MPa}} = 2.56 \quad (8)$$

Center Beam

The 80/20 aluminum T-slot beam was modeled as a 91.44 cm (36 in) straight beam fixed at both ends. The beam received a distributed load that was a sixth of the total 51.18 kN load that was predicted the test article would experience. The material for 80/20 is normally 6063-T5 aluminum but modeled as 6061 alloy as it is within the SolidWorks inventory and retains very similar material properties. For the hand calculations of the bending stress, we assumed the beam to have a constant parabolic curve from end to end. In the FEA trial, while fixing both ends and adding a distributed load, the beam had a parabolic curve that was not constant throughout the beam's length.

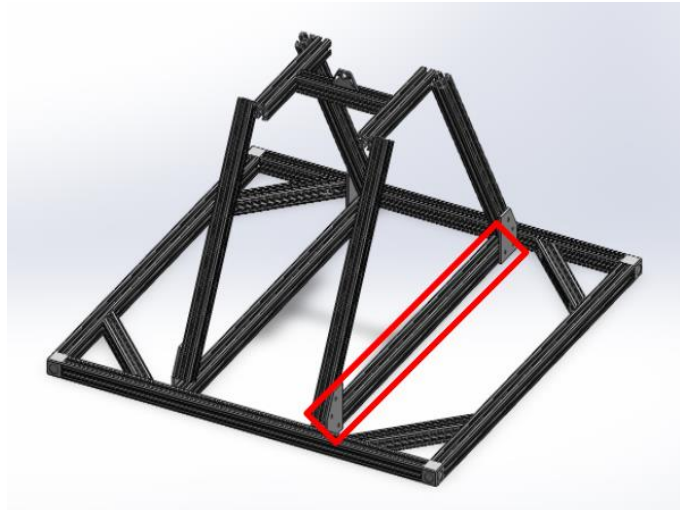


Figure 3.11: Analysis of a Fixed-Ends Beam

For the hand calculations of the bending stress, we assumed the beam to have a constant parabolic curve from end to end. In the FEA trial, while fixing both ends and adding a distributed load, the beam had an inconsistent curve throughout its length. Below are the equations used to calculate the maximum bending moment and bending stress of the centrally located beam previously identified.

$$\sigma_b = \frac{My}{I}$$

σ_b – Bending stress

M – Calculated bending moment

y – Vertical distance away from the neutral axis

I – Moment of inertia around the neutral axis

$$M = \frac{wL^2}{8} \quad (9)$$

$$M = \frac{53.25 \text{ N/m} * 36^2}{8} \quad (10)$$

$$M = 974.92 \text{ N} - \text{m} \quad (11)$$

$$\sigma = \frac{My}{I} \quad (12)$$

$$\sigma = \frac{974.92 \text{ Nm} * 1.91 \text{ cm}}{85.74 \text{ cm}^4} \quad (13)$$

$$\sigma = \mathbf{171.69 \text{ MPa}} \quad (14)$$

For our calculations, we found the maximum bending moment to be 974.92 N-m and a maximum bending stress of 171.69 MPa. After reaching these values, we then designed an FEA simulation to simulate the same bending moment as calculated above. The goal of the FEA was to get as close as possible to matching the two sets of values for the moment and bending stress.

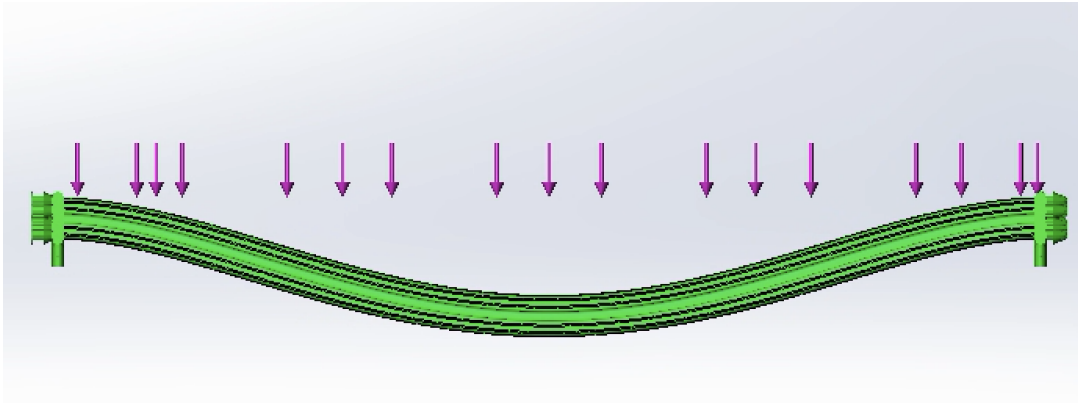


Figure 3.12: Distributed Load, Fixed-Ends Beam

As seen in *Figure 3.12*, the max bending stress is 109.27 MPa, which is within the same factor as the hand calculation. The next steps in the process were identifying where the FEA differs from the simplified model for hand calculations and working towards finding verification that the calculations match. Additionally, the resolution of the mesh and specifics of running the simulation also contribute to varying answers within what looks to be a straightforward simulation. This exercise has exposed us to the various ways FEA can be used on a part or a whole assembly, and often needs someone who is proficient in their understanding of traditional FEA and has a deep understanding of how the software interacts with the digital model.

3.5 Data Acquisition:

To record data during the drop tests, the YostLabs 3-Space Bluetooth accelerometer was chosen due to its high-g range, gyroscopic capabilities, and ease of use through Bluetooth (Datasheet on *Appendix E*). Three accelerometers were purchased so they could be placed on different points of the frame to assess impacts, rotations, and rebounds more accurately before, during, and after impact. The first accelerometer was placed in the center of the system to get a reading of how the system behaves, the second accelerometer was placed above a crumple column to read how the columns behaved upon impact, and the final sensor was placed on one of the outer edges, where system rotation would be most prevalent.

The accelerometers were set to record corrected, linear, and raw acceleration, as well as rotation. The corrected acceleration was expected to produce a filtered signal that would produce an easily interpretable curve. The linear acceleration would help more easily compare the data to that of the orientation changes. Raw acceleration was recorded to have the base values that could be referenced during analysis if needed.

Chapter 4: Manufacturing & Assembly

4.1 Manufacturing Plan and Procurement

After choosing a final design, the team began ordering parts for the manufacturing of the vehicle. The Outer Frame subsystem was chosen to be the first one to be manufactured because it will serve as the backbone of the vehicle. The frame was designed to be mainly built of modified off-the-shelf components. This would allow for simpler assembly and modifications if necessary. Once the frame was complete, the crumple columns were assembled. Each column is composed of acrylic plates, nine wooden dowels with a half-inch diameter, and 36 aluminum cans.

The aluminum rails making up the frame and their corresponding fasteners were purchased from McMaster-Carr. Scrap ¼-inch acrylic sheets from the machine shop were used for the crumple columns. The wooden dowels were purchased in bulk from a local hardware store to minimize their cost. The 144 aluminum cans were donated by other students.

4.2 Machining

Frame

The aluminum rails were cut to length using a band saw and faced on a vertical mill. The ends of the rails making up the base were tapped using a hand drill. The rail that would support the entire assembly when suspended during testing was tapped and drilled into to accommodate the eye bolt the rope would tie to. The aluminum plates that held together the top of the frame had seven holes drilled into them with a vertical mill to allow for a connection to the frame and eye bolt rail.

Crumple Columns

The acrylic sheets were laser cut to eight-inch squares and to have nine holes the dowels would go through. The dowels were then cut to length using a miter saw. In the meantime, each individual aluminum can had ½-inch holes drilled into the top and bottom faces.

4.3 Assembly

Frame

The frame was assembled by connecting the 80/20 aluminum bars using a variety of mounting brackets and T-nuts and bolts, shown in *Figure 4.1*. The aluminum plates that held the diagonal beams to the load-bearing eye bolt beam were bolted to the top of the frame. The eye-bolt beam was fixed between the two aluminum plates.



Figure 4.1: Assembled Base of Frame

Crumple Columns

The crumple columns were assembled by feeding four cans through each of the 36 wooden dowels. The can-dowel assemblies were fed through the holes of the acrylic plates to make four groups consisting of 36 cans and nine dowels with an acrylic plate on each end. The top end of these crumple columns was then fixed onto the bottom of the four corners of the frame with T-nuts and bolts.



Figure 4.2 Assembled Leg (left), Attached to Frame (right)

4.4 Test Assembly & Setup

The Ground Support Equipment (GSE) was set up next to a grounded vertical railing (fixed end) support. This location allowed for the cantilever to minimize any potential yaw motion due to human-rope lifting action. Plastic cable ties were calculated to support 40 in-lbs. from the cantilever moment and prevented the yaw motion.

Accelerometers were connected, calibrated, and tared; cans were further secured from any falling out via tape adhesive; human climbing rope was secured via bowline knot and fed through the cantilever pulley up to the designated lift team.

Chapter 5: Design for Testing

5.1 Ground Support Equipment

In performing a physical drop test, reliable and effective GSE was necessary to maintain viable and accurate results. The GSE chosen to support and guide the vehicle was a 62.5x8.9x8.9 cm (LxWxH) Douglas Fir cantilever beam. The beam utilized a single 45° (3.8x8.9 cm; WxH) wood brace for extra bending rigidity. A cantilever was identified as the quickest and simplest manufacturable method for guiding a load over a railing supported on a second story balcony. The railing was identified per OSHA guidelines [4] to support a top load of 90.71 kg, which was strong enough to support the moment and point loads from the cantilever.

The vertical portion of the cantilever beam setup was attached to the vertical railing with cable ties, which countered a 30.5 kg-m moment. The cord used to support, lift, and drop the test article was a rock-climbing rope, which can hold the weight of a small person, similar to the 54.43 kg of the test article. The pulley and cord were utilized to lower the force required to lift the load, while also guiding the test article upon drop. The electronics onboard for testing were the Bluetooth accelerometers, which were calibrated, tared, and actively recording in preparation for the drop (or any accidental premature drop) when the test article was suspended.

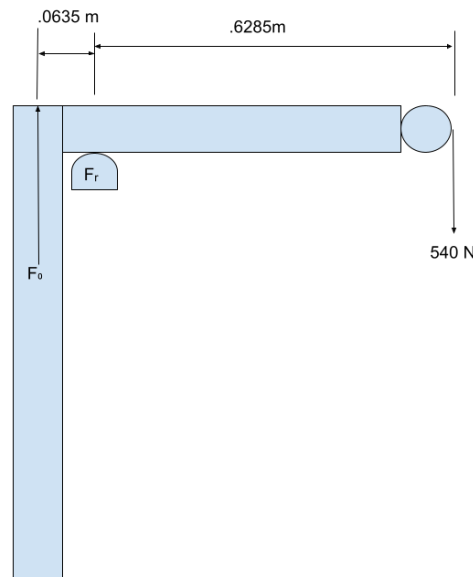


Figure 5.1: Two-Dimensional Example of Cantilever Test Setup

In *Figure 5.2*, the acting forces present are F_o and the 540 N vehicle load. The support F_r represents the railing as a rocker support. The cantilever beam acts in a seesaw manner using F_r as

the rocker. In this scenario, the fasteners supporting the load F_0 experience a 544.37 kg upward force.

$$F_0 = \frac{55kg \cdot 0.6285m}{0.0635m} = 544.37kg \quad (15)$$

To find the bending stresses and deflection under load, the following were found:

Area moment of inertia:

$$I_x = \frac{bh^3}{12} = \frac{0.089 \cdot 0.089^3}{12} = 5.229 \cdot 10^{-6} m^4 \quad (16)$$

Deflection in the beam:

$$\delta = \frac{PL^3}{3EI} = \frac{540 \cdot 0.6285^3}{3 \cdot 13444 \cdot 10^6 \cdot 3.268 \cdot 10^{-7}} = 0.01m = 1cm \quad (17)$$

According to Table 4-3a in *Wood Handbook – Wood as an engineering material*, the modulus of longitudinal Elasticity for an interior West Douglas Fir (12% moisture content) is $E=12,600$ MPa [5]. This value was used to calculate the max deflection of the beam, which was estimated to be 1 cm. The actual deflection in the test was negligible. The max bending stress of the beam showed it to be 5.78 MPa.

$$\sigma_{max} = \frac{M \cdot y}{I} = \frac{(540 \cdot 0.6285) \cdot 0.089}{5.229 \cdot 10^{-6}} = 5.78 MPa \quad (18)$$

When compared to the wood's maximum allowable parallel bending stress of 8.9 MPa, a bending factor of safety of $n = 1.54$ was found. The actual test setup in its final state is shown below.

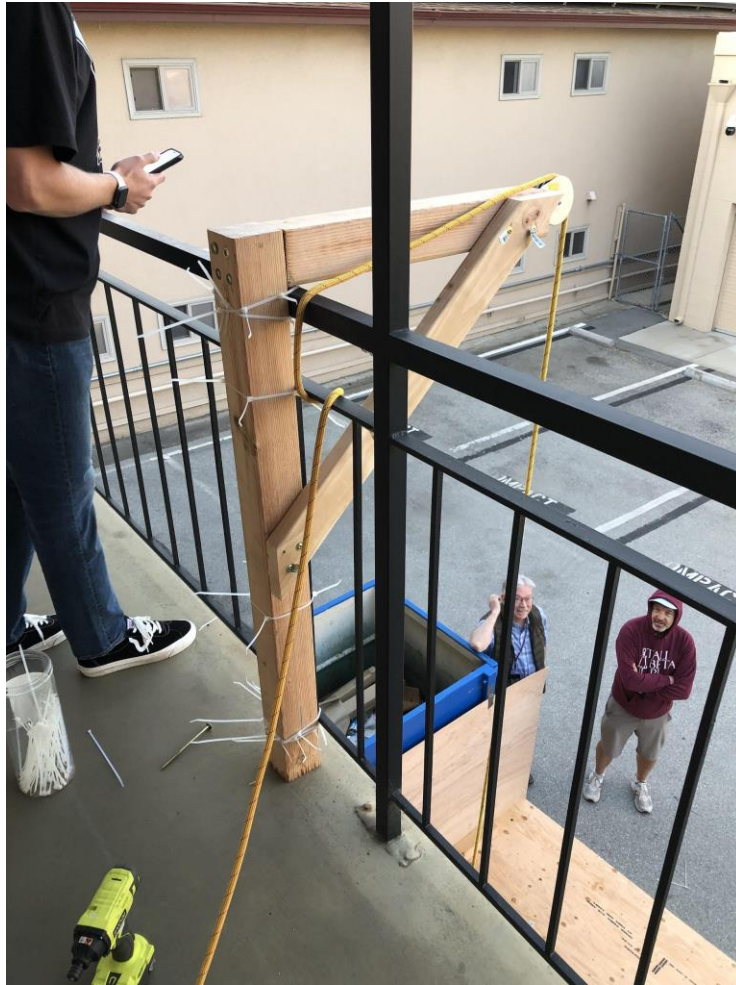


Figure 5.2: Image of Actual Ground Support Equipment Setup

5.2 Safety & Procedure

To conduct the physical drop test, several safety concerns needed to be addressed. Chief among these was the possibility for portions of the test article to be ejected and become hazardous projectiles as the impact is absorbed upon contact with the ground. To mitigate this risk, a small apartment complex (733 Benton St.) and its parking lot were closed to the public and protective walls were constructed from plywood to surround the drop area and contain any resulting shrapnel. Furthermore, two additional sheets of plywood were laid on the ground to serve as the impact surface for the drop test. This ensured not only that the surface of the lot was not damaged by the falling test article, but also that the landing zone was as level and uniform as possible. As an added precaution, all who were present were required to wear safety glasses at the time of the drop. Our safety setup provided shrapnel protection to three sides of the square landing zone, leaving one open for filming, and protected the parking lot surface from impact damage.

The drop test was conducted using a designed cantilever support arm affixed to the railing of the second-floor balcony at 733 Benton St. The cantilever extended over the drop zone far enough to prevent any interference with the crash vehicle by the building and curbs below. The support arm was fixed to the railing using a combination of rope and zip ties and distributed the weight of the test article into the floor of the balcony and as a torque on the railing. At the end of the arm, a pulley was fixed to guide the test article as it was raised and dropped by means of a climbing rope. To conduct the test, accelerometers were fixed to the test article, paired with present computers, and tared while the assembly was on the ground. Using a bowline knot, the rope was tied to the test article and used to raise it to the desired height by means of the pulley on the cantilever arm. Once elevated, slow-motion cameras were activated, pointing at the drop site, accelerometer recording was initiated, and the test article was released from the balcony. Immediately following the drop, the amount of deflection by the cans was measured and recorded along with the resulting accelerometer numerical data and plots.

Chapter 6: Test Results & Analysis

6.1 Drop Tests One and Two Results

The first drop test of the article was conducted using 144 total cans (arranged in a matrix of 3x3x4 on each of the four legs) and dropped from a height of 2.44 meters with a total system mass of 31.75 kg. One main goal of this drop test was to measure the deflection of the frame and crumple distance of the crumple columns, and ultimately determine the impact response behavior of the aluminum cans. Similarly, we planned to measure acceleration data using our accelerometer for further analysis.

Upon impact, the crumple zone system exhibited a small amount of plastic deformation. The load frame exhibited significant elastic deflection inwards towards the centerline of the frame during ground contact, as can be seen in *Figure 6.1*. After reaching its maximum point of compression, the entire system rebounded 15 cm above the ground before coming to rest. Upon inspection of the crash vehicle following the first drop, no signs of damage or plastic deformation to the frame were observed.

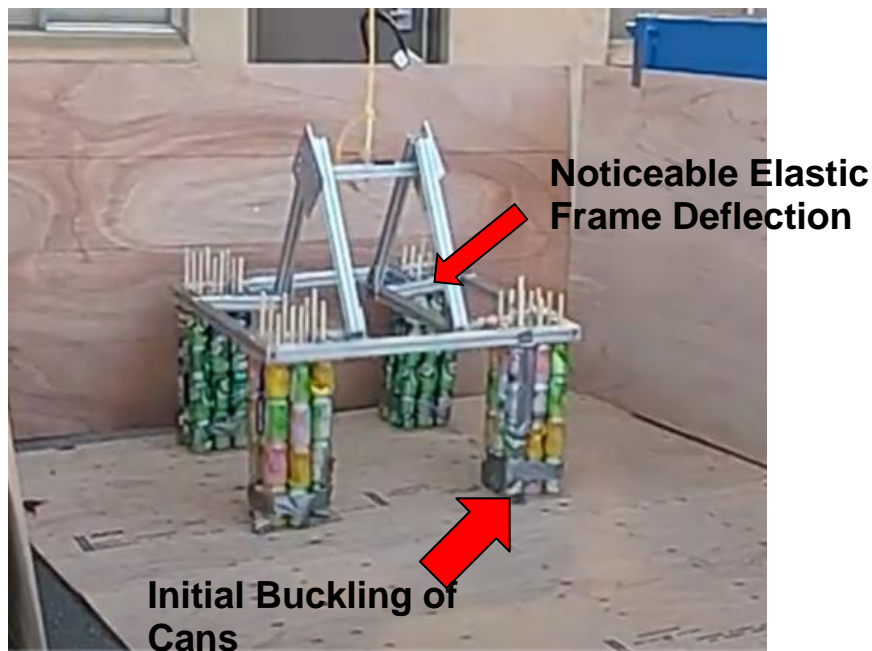


Figure 6.1: Live Image Taken Immediately Following Initial Impact of Test One



Figure 6.2: Test Article's State After First Two Drop Tests

Because the crumple zone exhibited minimal deformation following the first drop test, a second test was conducted under the exact same conditions, without replacing any of the crumple zone. This second drop test yielded similar results as the first, with approximately 15cm of rebound following impact and no observed damage or plastic deformation to any parts of the system apart from the crumple zone. Following these two tests, each crumple zone leg experienced a total of 9.84cm of crumpling on average. The crumple zone was then taken apart for further examination and analysis, and it was determined that 72 out of the 144 total cans were significantly crumpled through at least half of their travel (change in height of approximately 7.62cm), with 64 cans remaining completely unyielded. Therefore, 80 out of the 144 total cans can be attributed to absorbing the impact via plastic deformation and cylindrical buckling.

Regarding the data collected during each test, a single accelerometer was mounted to the top of the load frame adjacent to the drop hook. The data was sampled from the accelerometer via 2.4 GHz Bluetooth at a resolution of 12 bit and sampling rate of 250 Hz. After the test article was dropped, the acceleration of the article was recorded by the accelerometer and the measurements can be seen in the following figures.

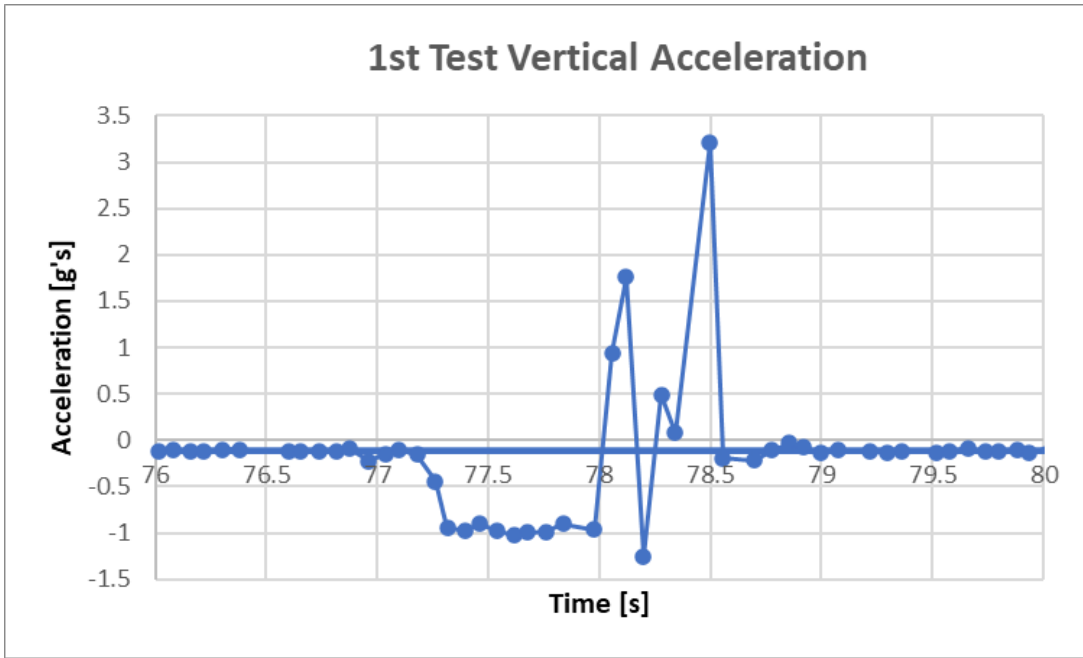


Figure 6.3: Accelerometer Data from Drop Test One

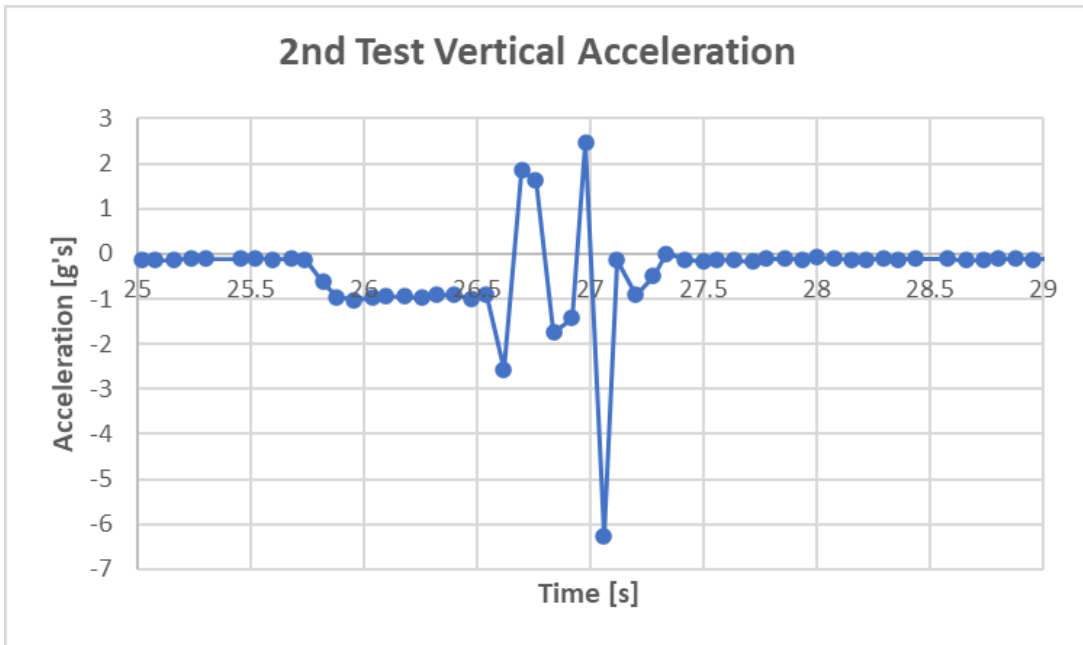


Figure 6.4: Accelerometer Data from Drop Test Two

As depicted above in Figures 6.3 & 6.4, it can be observed that the maximum acceleration recorded for the first drop test was 3.21 g's upwards while the maximum acceleration recorded for the second drop test was 6.28 g's downwards. Standing alone, these numbers appear quite satisfactory as the system was designed to withstand acceleration upwards of 30 g's. However,

looking at the data graphs the recorded acceleration response was quite sporadic. The second test accelerometer data displaying its maximum acceleration downwards right before coming to rest further suggests that the recorded accelerometer data does not match the kinematic behavior of the system's center of mass that was observed in slow motion video recorded of the tests. There are two factors that were identified as being responsible for this phenomenon.

First, the location of the recording accelerometer at the top of the frame contributed to the accelerometer recording significant oscillations that could be observed throughout the frame upon inspection of the recorded slow-motion video of the impact. These oscillations occurred because of the elastic behavior of the aluminum frame members.

Secondly, examining the number of data points recorded by the accelerometer over a 1 second time interval it is apparent that the accelerometer recorded data at a rate of only 14 Hz. This was quite surprising because the accelerometer was set to a sampling rate of 250 Hz before the test was conducted. Following inspection of the recorded data in conjunction with independent experimental testing of the accelerometer sampling rate, it was determined that the accelerometers utilized a built-in filtering mechanism that reduced the processed resolution of the recorded data. The accelerometer manufacturer was contacted but were unfortunately unable to resolve the issue. However, it was determined that a sampling rate of 52 Hz was able to be achieved using a wired connection of the accelerometer to a computer. This strategy was utilized in drop test three.

Due to these circumstances, no conclusions about the kinematic behavior of the system's center of mass could be reached when analyzing the accelerometer data recorded during these two tests.

6.2 Drop Test One and Two Analysis

Following drop tests one and two, it was concluded that the plastic deformation exhibited by the crumple zone was marginally less than anticipated, and the amount of rebound that occurred after impact was an indication that the system exhibited an unsatisfactory amount of elastic response to the impact. In other words, energy that was designed to be absorbed by the plastic deformation of the crumple zone was instead stored elastically through various aspects of both the load frame and the crumple zone. Nonetheless, the following calculations were used to determine the average amount of energy absorbed by each can in the crumple zone across the two tests.

$$E_{absorbed} = mgh_d - mgh_r = mg(h_d - h_r) \quad (19)$$

$$E_{absorbed} = 31.75 \text{ kg} * 9.81 \text{ m/s}^2 * (2.44 - .15 \text{ m}) = 713.26 \text{ J} \quad (20)$$

$$E_{absorbed,can} = \frac{2 \text{ drops} * 713.26 \text{ J}}{80 \text{ cans}} \quad (21)$$

$$E_{absorbed,can} = 17.83 \text{ J} \quad (22)$$

As shown above, the average amount of energy absorbed by each crumpled can upon impact was estimated to be 17.83 J using a simple application of the gravitational potential energy equation. This value greatly differs from the value obtained during our preliminary drop test of the 20.4 kg mass from a height of 2 m, which absorbed approximately 47 J of impact energy per can. Upon inspection following the initial two drop tests of the crash article, it was determined that there were several factors that contributed to the deviation in performance of the crumple zone from what was originally anticipated.

The first and primary factor identified in contributing to this discrepancy is the difference in amounts that the cans were crumpled on average. It can be intuitively understood that if a can is only crumpled one third of its travel, then it will have only absorbed somewhere near one third of its maximum potential energy. In the preliminary drop test, all 8 of the cans used were crumpled entirely through their linear travel, while many of the cans used in drop tests one and two were only partially crumpled after the tests and 64 showed no signs of plastic deformation. If the above calculation is then redone and the energy absorbed is attributed across all 144 cans present during these tests, then the energy absorbed is determined to be 9.91 J per can across both tests, and 4.65 J per can per test.

Another contributing factor to the discrepancy in quantifying per can energy absorption, is energy losses due to friction between the dowel rods and their acrylic guide plates. After testing, it was noticed that the tolerance stacks up between the wooden dowel rods and acrylic guide plates in the crumple zone was insufficient such that significant friction was present when the rods telescoped through the acrylic guide plates. The amount of friction between these two surfaces was especially significant when subjecting the dowel rods to slight angles of deflection away from perfect orthogonality to the plates. In these cases, the rods could not telescope freely through the guide plates and therefore likely served as a major contributor of unanticipated friction losses during the impact absorption of the test, as well as increased elastic response of the entire system. If it is the case that the dowels locked up with the guide plates during impact, then a significant portion of the impact load would have traveled directly from the ground through the dowels to the load frame, without

first passing through the crumple zone. This is what is identified as the most significant contributing factor to the oscillatory elastic response of the load frame that was recorded by the accelerometer and witnessed in video recording of the impact.

The third factor we determined to be a major contributor to the discrepancy between the expected and actual test result was an insufficient frame mass. For drop tests one and two, the total system mass was 31.75 kg, almost all of which can be attributed to the mass of the load frame, with the total added mass of the cans and dowels assumed as negligible. With a greater sprung mass, the crumple zone would exhibit much more use of its travel and therefore each can could use a greater amount of its energy absorption potential (upwards of 50 J as determined by preliminary testing).

6.3 Drop Test Three Results

After completing the first two drop tests and analyzing their results, the team decided to complete a third drop test with several modifications to the configuration with the intention of correcting the unexpected phenomena, as well as obtaining more qualitative and quantitative data for the experiment so that more refined conclusions could be made. The changes made to the system and test setup are as follows. For the third test, three accelerometers were attached at various locations on the frame with the intention of allowing us to better understand both the kinematic response behavior of the total system as well as how elastic response behavior is affected by frame location. Furthermore, one accelerometer was equipped to the recording computer via USB cable to obtain the highest possible sampling rate of 52 Hz.

Regarding changes to the crumple zone, the total number of cans was reduced from 144 to 72 to ensure all the cans crumple completely. The results from this would more accurately represent how much energy the cans absorb. The holes in the cans and the acrylic plates were expanded to eliminate losses in the system due to friction between the wooden dowel rods. Additionally, 22.6 kg of mass was added to the frame to reflect the design calculations more accurately at 54.43 kg.

For the data collection of the second test, three accelerometers were placed at separate points along the frame to assess impacts, rotations, and rebounds more accurately before, during, and after impact. The first accelerometer was placed in the center of the system atop the frame (same location as drop tests 1 & 2) to get a reading of how the system behaves, the second accelerometer was placed above a crumple column to read how the columns behaved upon impact, and the final sensor was placed on one of the outer edges, where system rotation would be most

prevalent. The accelerometers were set to the Q-Comp setting, which would allow a theoretical maximum sampling rate of 1250 Hz. Two accelerometers transferred data through Bluetooth while the third was connected with a cable for reliability.

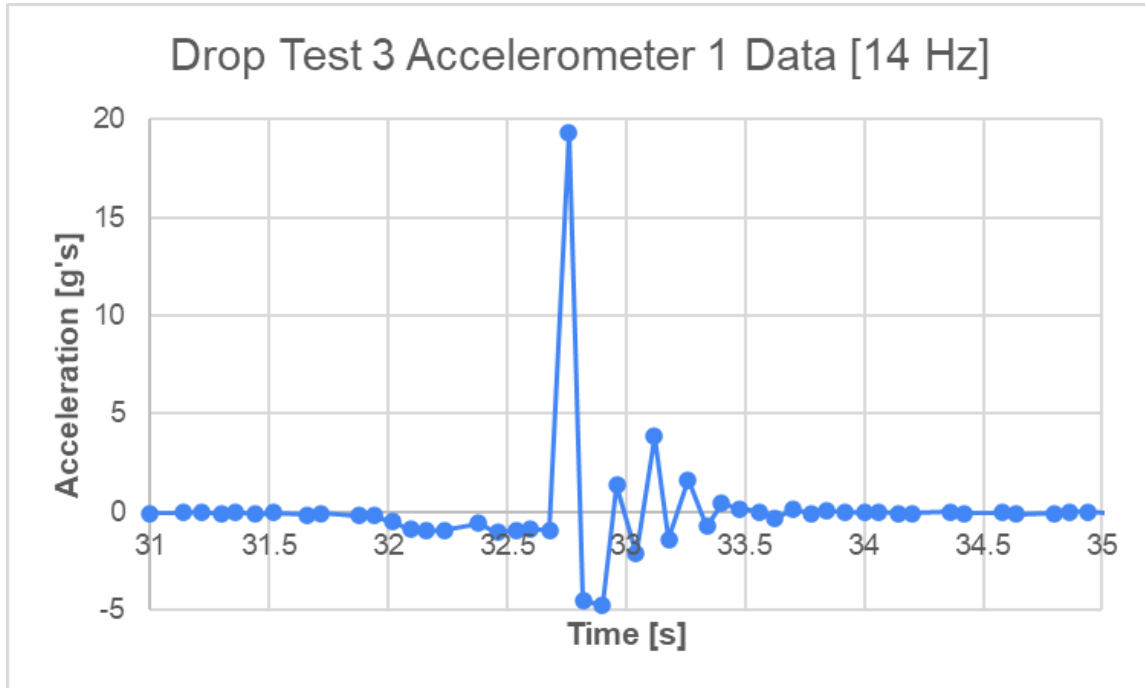


Figure 6.5: Accelerometer #1 Data from Drop Test Three

Accelerometer #1, which was located at the top of the frame, showed the max recorded acceleration is seen to be 19.34 g's with a data acquisition rate of 14 Hz. Accelerometer #2, which was located on the bottom part of the frame during the drop, had a maximum acceleration of 21.02 g's while running at 52 Hz. These results can be seen in *Figure 6.6*. Unfortunately, the data obtained from accelerometer #3 was unable to be retrieved following the test, which was attributed to a faulty Bluetooth connection.

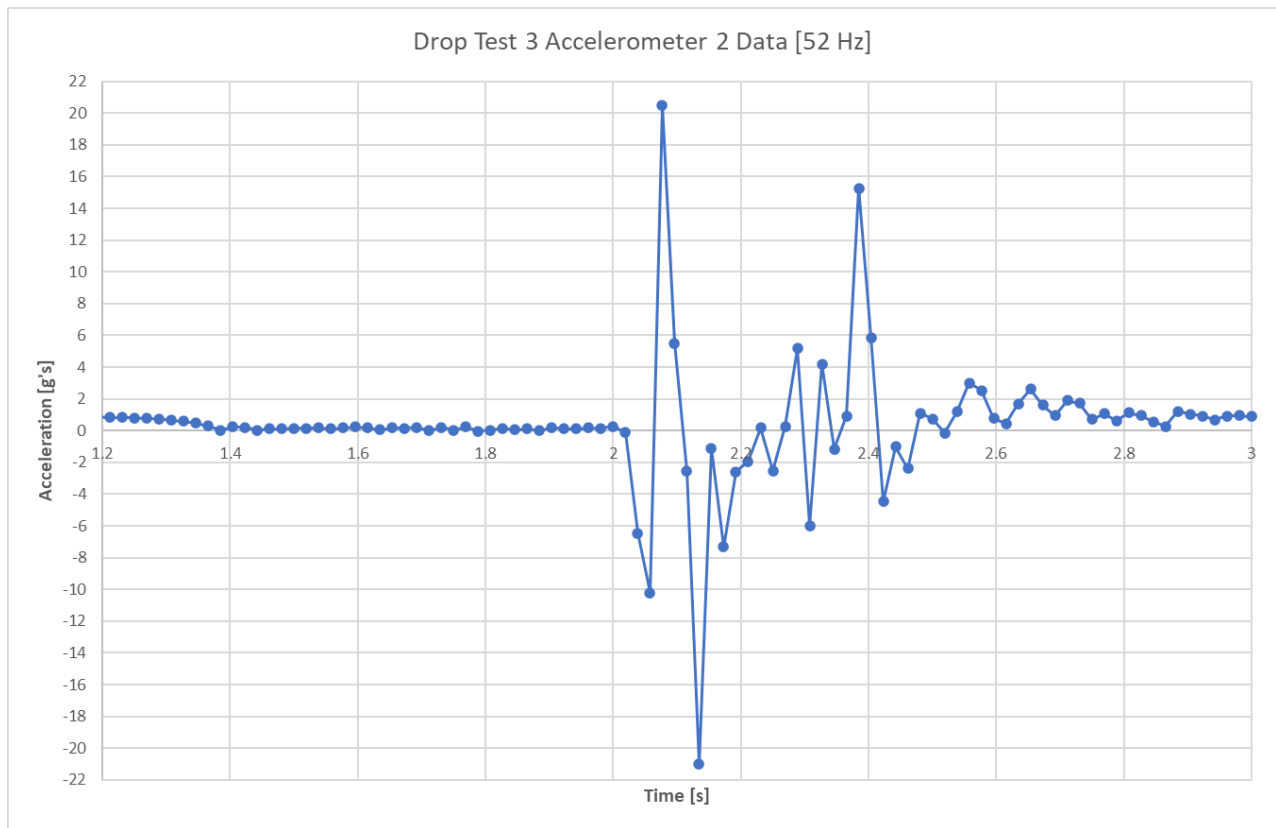


Figure 6.6: Accelerometer #2 Data from Drop Test Three

6.4 Drop Test Three Analysis

All the cans in the crumple zone were fully crumpled from the impact. The assembly underwent a maximum acceleration of 21.02 g's with no damage to the frame. From prior research, it was found that the NASA Opportunity Rover must be able to withstand 26.4 g's to pass the safety testing prior to launch. Since the maximum acceleration of our drop test was about 20% lower than that of the Opportunity Rover, the Rover should be able to remain completely intact using this design and testing conditions. Additionally, the system mass and energy absorption materials were designed at only 10% of the Opportunity Rover. The vehicle was able to withstand 80% of the goal acceleration with a crumple zone that was only designed to absorb 10% of the energy from the drop, therefore the deduction can be confidently made that a failure of the sky crane maneuver from at least 2.5 meters in the application of the Mars Perseverance mission should protect the rover from any damage.

Along with the data recorded by the accelerometers, we were also able to get much information from visual analysis of the crumple columns after the test. After conducting the drop

test, the height of the crumple columns decreased from 20.32 cm to 15.1 cm. During the first drop test with the four layers of cans, there was a 12% decrease in height. Because we added extra weight and removed half of the cans, the group was able to achieve a larger percentage of deformation in the cans. This percent deformation directly correlates to the amount of energy absorbed by each can.

Like the first drop test, the group was able to take the potential energy of the vehicle, using the drop height “ h_d ”, right before it was released to find how much energy would need to be absorbed by the cans. Also, because there was a small rebound after the drop, what we call “ h_r ”, we can calculate the total energy absorbed by the system by subtracting the two kinetic energies. This process is shown below.

$$E_{absorbed} = mgh_d - mgh_r = mg(h_d - h_r) \quad (23)$$

$$E_{absorbed} = 54.43 \text{ kg} * 9.81 \text{ m/s}^2 * (2.44 - .05 \text{ m}) = 1.275 \text{ kJ} \quad (24)$$

$$E_{absorbed,can} = \frac{1.275 \text{ kJ}}{72 \text{ cans}} \quad (25)$$

$$E_{absorbed,can} = 17.73 \text{ J} \quad (26)$$

After computing the energy that each can absorbed during the second drop, 17.73 J, the team compared this to the energy per can from the first drop testing. Considering we calculated 17.83 J per can in the first drop, our energy absorption in the third drop was very close to the previous measurement. Before testing, the team was anticipating an increase in the energy absorbed per can due to the fewer number of cans as well as the added mass of the system. Theoretically, with a higher mass and fewer cans to be crumpled, there would be more energy to be absorbed by the cans. Despite the changes made during the third drop test, the energy absorbed per can was still very close to the same from the first test.

During the first test, we dropped the vehicle twice without replacing any of the cans. This means that during the second drop, the system was already partially crumpled before the second drop. This made it difficult to analyze the crumple distance for a singular test, which is how the crumple columns were analyzed after the second round of testing. Also, because we only measured the crumple distance and the number of cans crushed after the second drop of the first round of testing, we used the assumption that an equal percentage of cans were crushed during the first drop as the second. For the third drop test, we only used half the number of cans, so it was a more accurate count of the crushed cans. The weight of the system in the second round was closer to our

goal weight of 50 kg. Unlike during the first and second drop tests, there was no need for assumptions on crumple distance and number of cans crushed. However, because the calculated energy per can were still so close (17.83 J versus 17.73 J), the team has determined the calculated values of energy absorbed per can from both rounds of testing are accurate.

6.5 Comparing Test Results to Goal

The goal of reaching 30 g's to simulate the same acceleration as the Spirit Rover's airbag landing vehicle was about 8 g's too low, reaching a maximum of 21.96 g's. Under this testing condition, however, the frame suffered no damage and the passive impact absorption systems functioned correctly. On the third test, all the aluminum cans experienced deformation and found no functioning errors with the revised manufacturing solutions (reducing burrs, increasing through-hole diameter, using more adhesive tape). Knowing the test article was fully intact after 3 drop tests with increasing kinetic energy (and reduced buckling potential energy) each time, the test results demonstrate a viable solution for landing a rover. The cost effective and modular design allows for efficient scaling up and necessary modifications, to the point where it could be feasible carrying a full size, 1000+ kg Mars Rover (as seen in *Chapter 9: Scaling Up the Design*).

Chapter 7: Cost Analysis

After the group had a clear vision of what we planned on making for this project, we began searching for materials that we would be able to use to construct the vehicle. An overarching goal that we kept in mind while selecting these materials was to find the most inexpensive ones available that would still operate within the criteria of the design. Below is the bill of materials the group purchased over the entire year.

Table 7.1 Bill of Materials

| Item | Amount | Cost per unit (after tax) | Total Cost |
|------------------------------------|---------------|----------------------------------|-------------------|
| T-Slotted Beam (80/20 Aluminum) | 29 ft | \$12.60 / ft | \$365.40 |
| Frame Brackets | 22 | \$16-18 | \$394.14 |
| Fasteners | 7 | \$4.48 | \$31.36 |
| Aluminum Cans | 144 | \$0.80 / can | \$115.20 |
| Yost 3-Space Accelerometer | 3 | \$338.32 | \$1014.95 |
| Douglas Fir Beams | 1 | \$5.96 | \$5.96 |
| Plywood Sheets | 5 | \$31.31 | \$156.54 |
| Pulley | 1 | \$30.67 | \$30.67 |
| Fasteners | 30 | \$1.48 | \$44.40 |
| Eye Bolt with Nuts | 1 | \$9.37 | \$9.37 |
| TOTAL | | | \$2187.95 |

When the group originally submitted the budget request, we received the requested \$2,457 to complete the project. Because we had decided to use more cost-effective materials for the shock

absorbing system of the crumple zone, such as aluminum cans, we were able to spend more money on accelerometers. This decision was made to allow for a closer look at the drop testing and be able to maximize the design of the crumple columns. However, we overestimated the damage that these accelerometers would endure during the testing and purchased three when we only needed one.

Another portion of the money spent was designated to the purchase and setup of the actual testing equipment. To comply with SCU Campus Safety guidelines, there were several pieces of material that were purchased to ensure a safe drop. For example, around \$160 of plywood was purchased solely as a debris barrier during the testing. These necessary supplies took money away from the implementation of other impact absorbing materials, such as struts, that we initially planned on using during the preliminary design.

Chapter 8: Engineering Standards and Realistic Constraints

8.1 Ethical Justifications

As the world's population continues to grow, we continually put more strain on Earth's finite natural resources. Eventually, we will need to turn to other planetary and extraterrestrial means of gathering resources. The project seeks to minimize mission losses as a result of landing failures, both preserving precious resources invested into extraterrestrial missions and expediting the timeline of these missions because of continued successes. In the event of a partial landing failure, the analysis seeks to prove that the remaining kinetic energy of the lander on planetary entry will be absorbed by the lander itself upon impact. This alleviates the need for the construction of a new lander/rover and equipment as well as the scheduling and fueling for an entirely new launch, saving resources and months, if not years, of time on the quest to explore other planets. This way, we can potentially supplement Earth's resources with those brought in from space and colonize other worlds sooner, to decrease the burden the large population and industrial facilities place on Earth.

8.2 Environmental Impact & Sustainability

During the time of the project, the team emphasized ethical and environmentally conscious decisions in every situation we have encountered. As engineers, it is important to not only consider those things that would be unethical, but to put even more emphasis on making the good ethical decisions during the project. Our design recognizes environmental practices and utilizes several reusable parts. The aluminum railing used to build the outer frame can be repurposed for later use. Also, the aluminum cans in the crumple columns can be recycled. The project contained very low waste and lots of recyclable materials.

8.3 Manufacturability

In fabricating the test article, it was concluded that the primary manufacturing challenge was the frame of the vehicle as it needed to be able to withstand high impact stresses for multiple tests. Furthermore, the goal of this project was to create a testing article, aiming for the manufacturing process to happen once. After the frame was built, it was reused during all three drop tests. Our design focused on cheap and readily available materials that would allow for ease of manufacturability. These materials, as well as other off-the-shelf materials, made it so most of

the manufacturing process was assembly. The team's access to the Santa Clara University machine shop and Maker Lab supplied all the necessary machines needed to manufacture our design.

8.4 Health and Safety

The ethics challenges regarding safety and risk are not of too much concern when regarding the “public” who could be using this test article. The targeted public users would be NASA or another national space agency, which is governmentally regulated and in the use of technically competent people. There is not any readily identifiable public of which will be unacquainted with this test article. The testing conditions for this product will have to be in a safe area free of any bystanders within ten feet, so we had to make sure that potential users are aware of the operating parameters we've set for using the crash vehicle test article. Through contacting SCU campus safety, we were able to ensure the area of the testing was secure from any bystanders. If this product were used in a full-scale extraterrestrial mission, the ethics implications would be how any byproducts would affect the composition and local environment wherever it would land. Luckily, there would be no users affected as its use would be physically remote.

Chapter 9: Scaling Up the Design

Taking this design into a practical application for a Mars Rover landing would require scaling up to handle the mass of a full-size Mars Rover from a real mission drop height. During NASA's recent Mars 2020 Perseverance Rover mission, there was a sky crane that lowered Perseverance from 20 meters using cables (this maneuver was also used for the Curiosity Rover).



Figure 9.1: Artist's Depiction of the Curiosity Rover's "Sky Crane Maneuver" [8]

In the contingent case of cable (or other) failure during this "Sky Crane Maneuver," the Rover would free fall and, upon impact, experience approximately $196g$'s and have to dissipate 76280.5 J of potential energy. Given the size of the Perseverance rover [11], each leg would require a $11 \times 10 \times 10$ aluminum can array for a total potential buckling energy of $78,232 \text{ J}$.

Chapter 10: Summary and Conclusions

10.1 Summary

The team successfully designed, manufactured, tested, and analyzed a test article that absorbed the impact of a drop test using a modular crumple zone. This project brought insight into the impact-absorbing capabilities of different amounts and arrangements of aluminum cans.

The test article successfully withstood three drop tests, using two different system masses (31 kg and 54 kg) and two different can amounts, 144 and 72. The frame did not show any visible signs of failure or fatigue, demonstrating reliability and durability. To scale up the design for practical use, the amount of cans needed would be 4400, which would be able to utilize ~76.5 kJ of buckling energy to withstand a 20 meter drop onto hard Martian soil.

10.2 Other Practical Uses

The Mars Rover Crash Vehicle can be used in other practical applications that require supply drop uses. For example, military airborne supply drops could utilize a modular crash vehicle in case of partial or whole failure of the parachute. Additionally, civilian needs could include dropping supplies to personnel in hard-to-reach settings. For example, expeditioners low on resources in remote locations. The shipping industry could also benefit from this crash vehicle. Supply aircraft could drop supplies faster and direct onto vessel surfaces.

10.3 Lessons Learned

Testing

Lessons learned from testing included the need for fixing accelerometer connectivity and sampling issues, shock wave transient pulse control, and reducing rebound. The accelerometers procured had the ability to reach 1250 Hz, however, when sampling via Bluetooth, a sampling rate higher than 14 Hz was not achieved. When sampling with a cable connection, the maximum sampling rate achieved was 52 Hz. For the shock wave transient pulsations, we learned about that phenomenon after researching why the first test's top and bottom layer of cans buckled a greater distance than the middle layers. We learned the shock waves from the bottom layer would send a "transient pulse of high pressure and high kinetic energy... as they propagate through condensed phases" [3]. The resulting conclusion was that the shock wave would most likely rebound at the bottom and top layers in an oscillating manner, sending more of the impact force through those

layers. Additionally, we concluded, once a can has been deformed slightly, it's more likely to continue buckling under continuous compression while the attached but unbuckled can will remain intact. Some future solutions that were envisioned were adding premature deformations, like dimples, to the middle layers. The dimpling would allow all the layers to experience a more linear buckling upon impact, therefore minimizing rebound and shock wave pulsation.

Manufacturing

When manufacturing the frame and crumple zone, a few phenomena occurred that were not predicted to impact the first drop test. When drilling the cans for the dowel through holes, a burr was left inside that was difficult to file down. During assembly and testing, the dowels required significant effort to push through the holes. Upon the drop test impact, we could assume some of the kinetic energy change was due to the resulting frictional heat, rather than entirely directed to buckling the cans. The tolerance on the holes in the acrylic was $+.002''$, which we later estimated could have been increased to $+.02''$ and allowed for a slip fit that still guided the dowels.

References

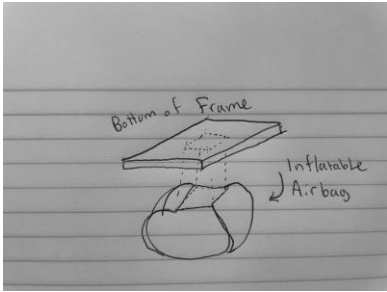
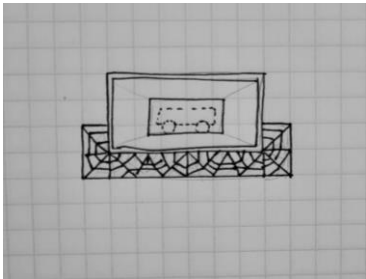
- [1] Anonymous 2020, "Choosing the ExoMars 2022 Landing Site,".
- [2] Billings, M., 2002, "Analytical Simulations of Energy-Absorbing Impact Spheres for a Mars Sample Return Earth Entry Vehicle”.
- [3] Douglas, A. S., 2014, "Mars Exploration Rover Airbag Landing Loads Testing and Analysis," 2022(Jan 29,).
- [4] Elert, M.L., Zybin, S.V., and White, C.T., 2005, "Chemistry at Extreme Conditions,"Elsevier, Amsterdam, pp. 351-368.
- [5] Galassi, T., 2013, "Requirements for Guardrail Systems".
- [6] Green, D.W., Winandy, J.E., and Kretschmann, D.E., 1999, "Wood Handbook - Wood as an Engineering Material,"U.S. Department of Agriculture, Forest Service, Madison, WI, pp. 1-45.
- [7] Harri, A., 2017, "The MetNet Vehicle: A Lander to Deploy Environmental Stations for Local and Global Investigations of Mars," Geoscientific Instrumentation Methods and Data Systems.
- [8] Hartman, A., Montgomery, H., Hereford, S., "Proof of Concept Planetary Lander Test Article".
- [9] National Aeronautics and Space Administration, 2017, "Curiosity's Sky Crane Maneuver, Artist's Concept".
- [10] National Aeronautics and Space Administration, "Entry, Descent, and Landing".
- [11] National Aeronautics and Space Administration, 2020, "Mars 2020/Perseverance".
- [12] NASA Jet Propulsion Laboratory, 2020, "Mars 2020 Perseverance Launch Press Kit".

[12] Xu, Q., Yang, Z., and Sun, Y., 2017, "Shock-Resistibility of MEMS-Based Inertial Microswitch Under Reverse Directional Ultra-High G Acceleration for IoT Applications," *Sci Rep* 7, (45512).

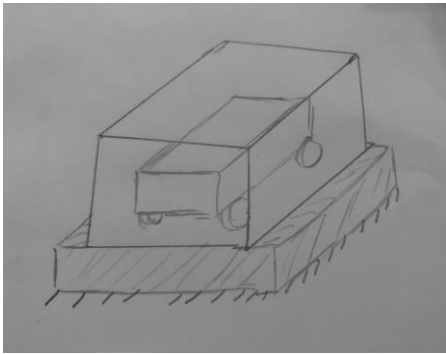
Appendices

Appendix A: Internal Concept Generation of Subsystems

During the Conceptual Design stage of our project, the group generated several different sketches for ideas on how to build the different subsystems. Once several designs were sketched, our team used a selection matrix (discussed above) to choose the design we were going to move forward with. This appendix illustrates sketches that we did not select to scale up for our project.

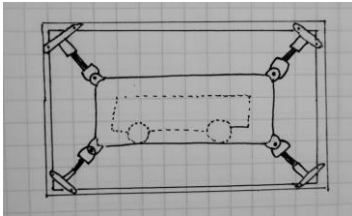
| Crumple Zone Subsystem | |
|---|---|
|  | <p>Air Bag</p> <p>Upon impact, gas-inflated fabric bags will deploy to quickly absorb and dampen the impact. This method is very fast and effective and is reusable.</p> |
|  | <p>Cell Structure</p> <p>A crushable metallic cell structure will permanently deform to absorb the impact. While this type of crumple zone is incredibly effective, it is complex and expensive due to its one-time use.</p> |

Inner Vessel Subsystem



Foam Barrier

A foam barrier beneath the rover will absorb residual impact force. Momentum will be eliminated as the foam compresses. The foam is effective but difficult to scale for heavier loads and faster descents.



8 Corner Shocks

Spring-based shock absorbers connect each of the corners of the Inner Vessel to the corners of the outer frame. The Inner Vessel is fully suspended and will oscillate in every direction to absorb the impact. This method is secure but expensive and complex.

Appendix B: Photos of Different External Designs Researched

Like Appendix A, this appendix highlights the researched external ideas that were discussed as possible designs for our subsystems. Several previously existing solutions were useful to get a better understanding of impact absorption techniques.

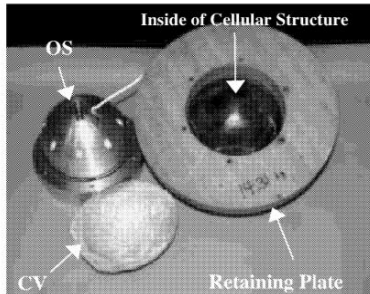


Figure 6 – Picture showing components of impact test specimen.

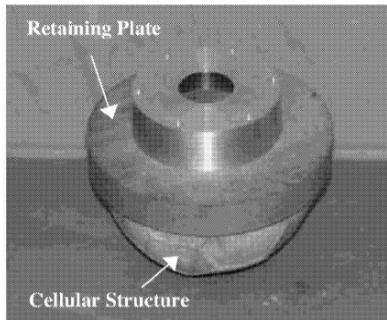
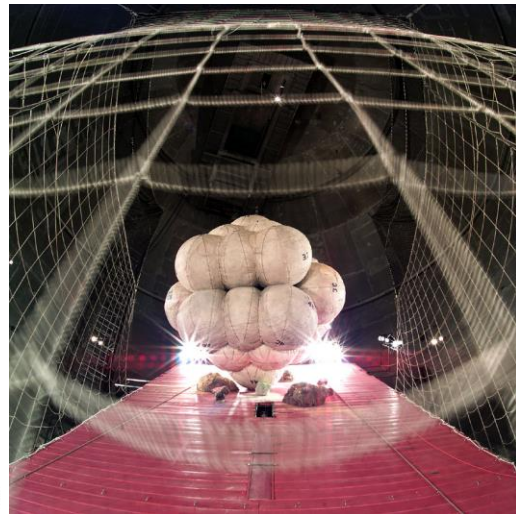
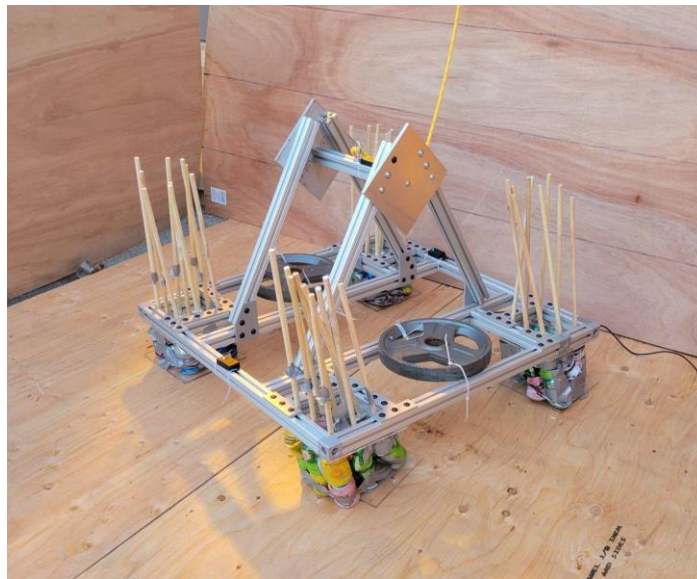
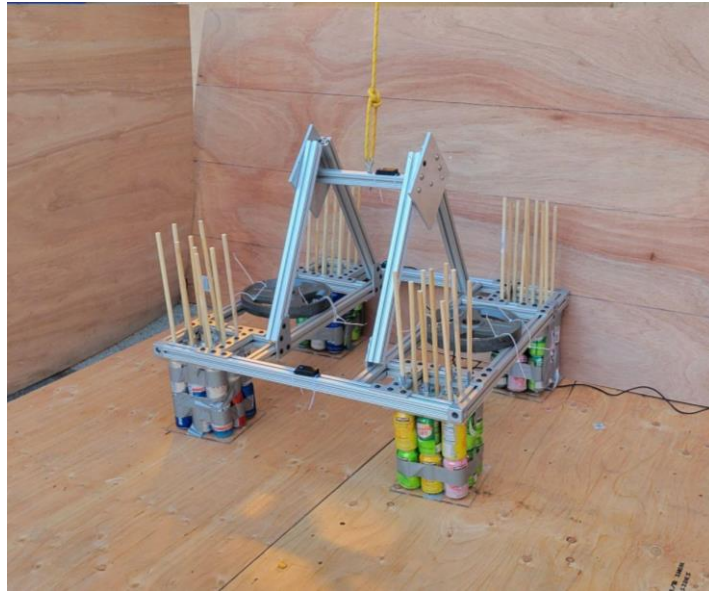


Figure 7 – Picture of typical impact test specimen with OS located within cellular structure.



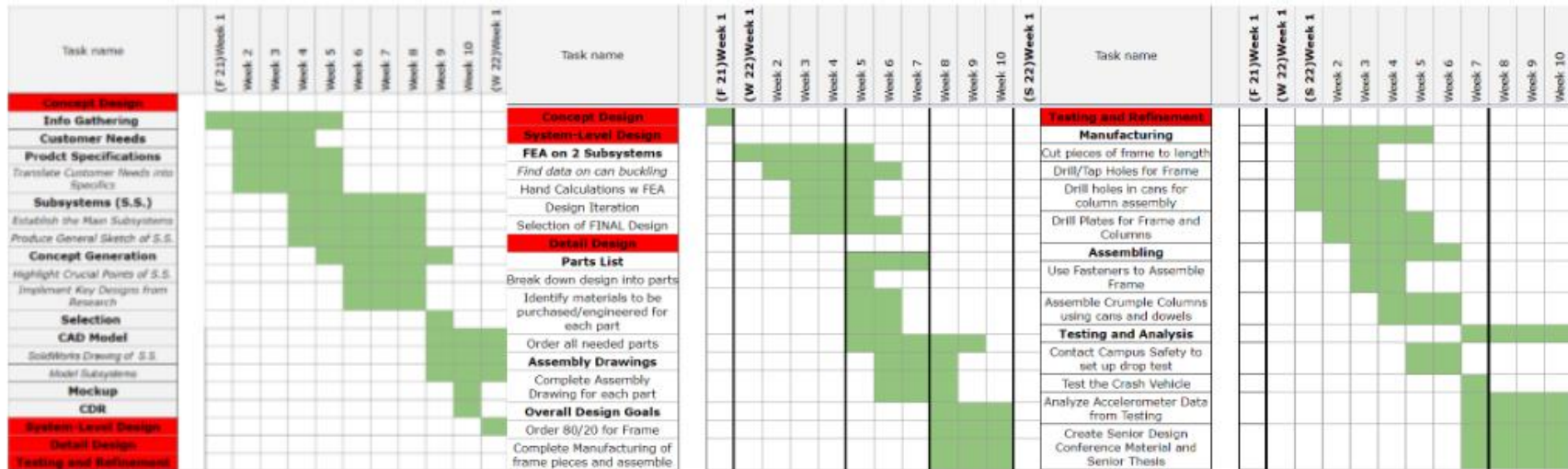
Appendix C: Photos of System

Before and after photos of the third drop test. As previously highlighted, there are only two layers of cans on each leg as opposed to the four layers tested the first two times. Also, the added weights and accelerometers can also be seen.



Appendix D: Timeline and Gantt Chart

Over the course of the school year, the team kept track of different deadlines and goals on a Gantt chart. This chart allowed us to map out the workload and manage the required tasks through the year.

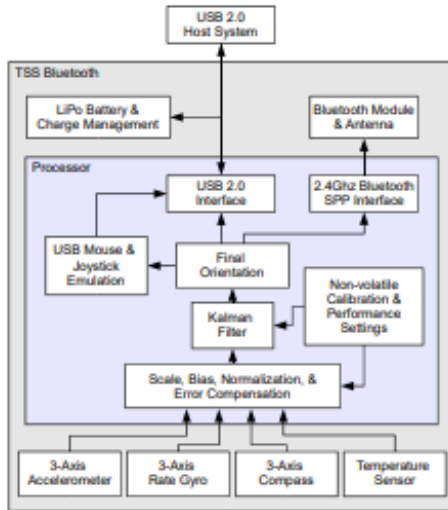


Appendix E: Accelerometer Datasheet

3-Space Sensor™ Bluetooth Miniature High-Performance AHRS / IMU Systems

High-reliability MEMS technology combined with advanced processing and multiple quaternion-based filtering algorithms allows for accurate orientation outputs across a wide range of performance conditions.

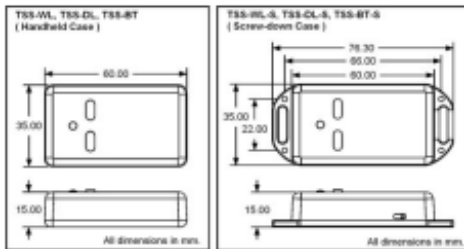
Block Diagram



Hardware Overview



Case Dimensions



Specifications

| General | |
|---------------------------------------|--|
| Part number | TSS-BT (Handheld Sensor Unit) TSS-BT-S (Screw-down Sensor Unit) |
| Dimensions | 35mm x 60mm x 15mm (1.38 x 2.36 x 0.59 in.) |
| Weight | 28 grams (0.98 oz) |
| Supply voltage | +5v USB |
| Battery technology | rechargeable Lithium-Polymer |
| Battery lifetime | 5+ hours continuous use at full performance |
| Communication interfaces | USB 2.0, 2.4GHz Bluetooth SPP (FCC Certified) |
| Wireless communication range | up to 300' (Bluetooth v2.0+EDR, Class 1) |
| Filter update rate ¹ | up to 250Hz with Kalman AHRS (higher with oversampling) up to 850Hz with QCOMP AHRS (higher with oversampling) up to 1350Hz in IMU mode |
| Orientation output | absolute & relative quaternion, Euler angles, axis angle, rotation matrix, two vector |
| Other output | raw sensor data, corrected sensor data, normalized sensor data, temperature |
| Shock survivability | 5000g |
| Temperature range | -40C - 85C (-40F - 185F) |
| Sensor | |
| Orientation range | 360° about all axes |
| Orientation accuracy ² | ±1° for dynamic conditions & all orientations |
| Orientation resolution | <0.08° |
| Orientation repeatability | 0.085° for all orientations |
| Accelerometer scale | ±2g / ±4g / ±8g selectable for standard models ±6g / ±12g / ±24g selectable for HH models ±100g / ±200g / ±400g selectable for H3 models |
| Accelerometer resolution | 14 bit, 12 bit(HH), 12 bit(H3) |
| Accelerometer noise density | 99µg/√Hz, 650µg/√Hz(HH), 15mg/√Hz(H3) |
| Accelerometer sensitivity | 0.00024g/digit-0.00096g/digit 0.003g/digit-0.012g/digit(HH) 0.049g/digit-0.195g/digit(H3) |
| Accelerometer temperature sensitivity | ±0.008%/°C, ±0.01%/°C(HH, H3) |
| Gyro scale | ±250±500±1000±2000 °/sec selectable |
| Gyro resolution | 16 bit |
| Gyro noise density | 0.009°/sec/√Hz |
| Gyro bias stability @ 25°C | 2.5°/hr average for all axes |
| Gyro sensitivity | 0.00833°/sec/digit for ±250°/sec 0.06667°/sec/digit for ±2000°/sec |
| Gyro non-linearity | 0.2% full-scale |
| Gyro temperature sensitivity | ±0.03%/°C |
| Compass scale | ±0.88 Ga to ±8.1 Ga selectable (±1.3 Ga default) |
| Compass resolution | 12 bit |
| Compass sensitivity | 0.73 mGa/digit |
| Compass non-linearity | 0.1% full-scale |

1. Depends upon communication mode, filter mode, Bluetooth adapter
2. Average value when calibrated
Specifications are subject to change
Version: 2.2.1

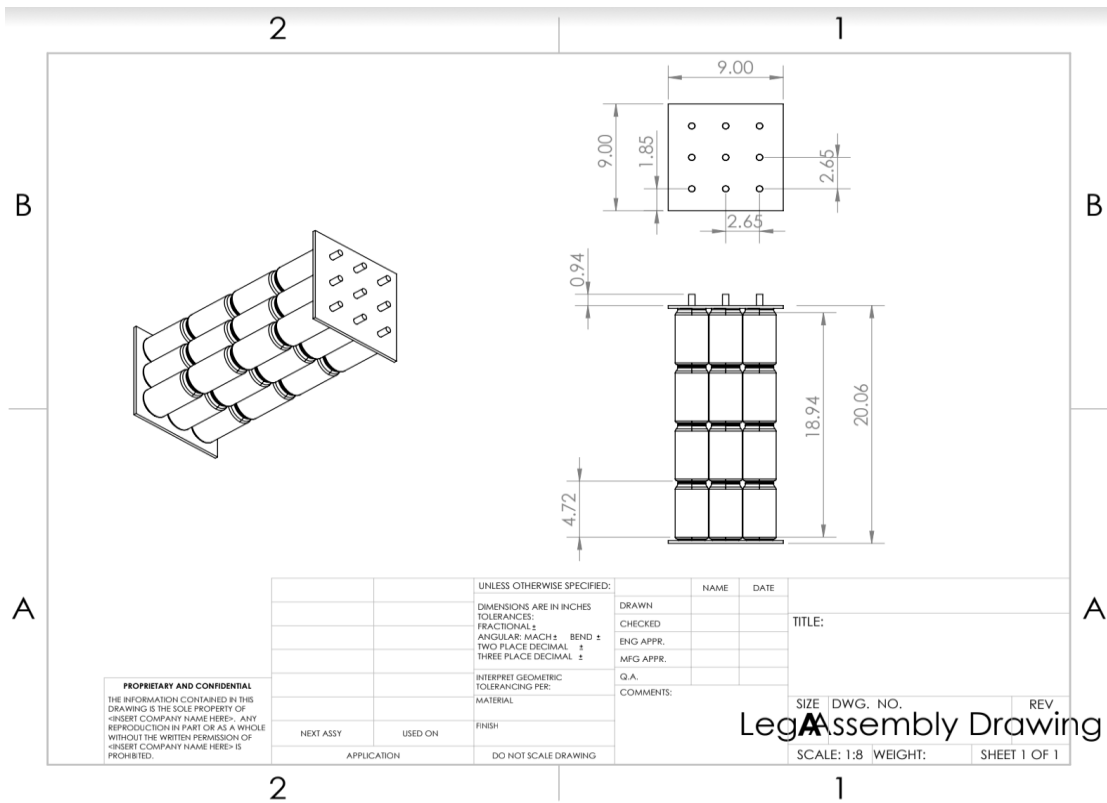
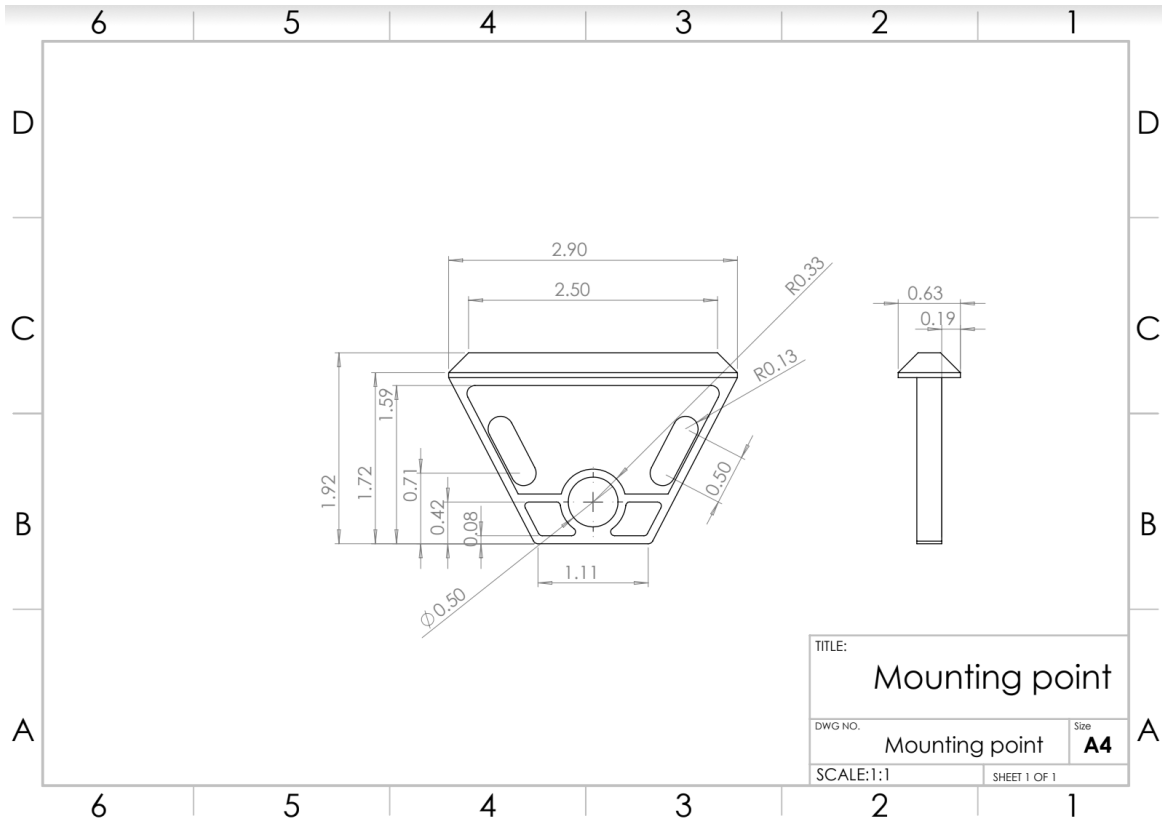


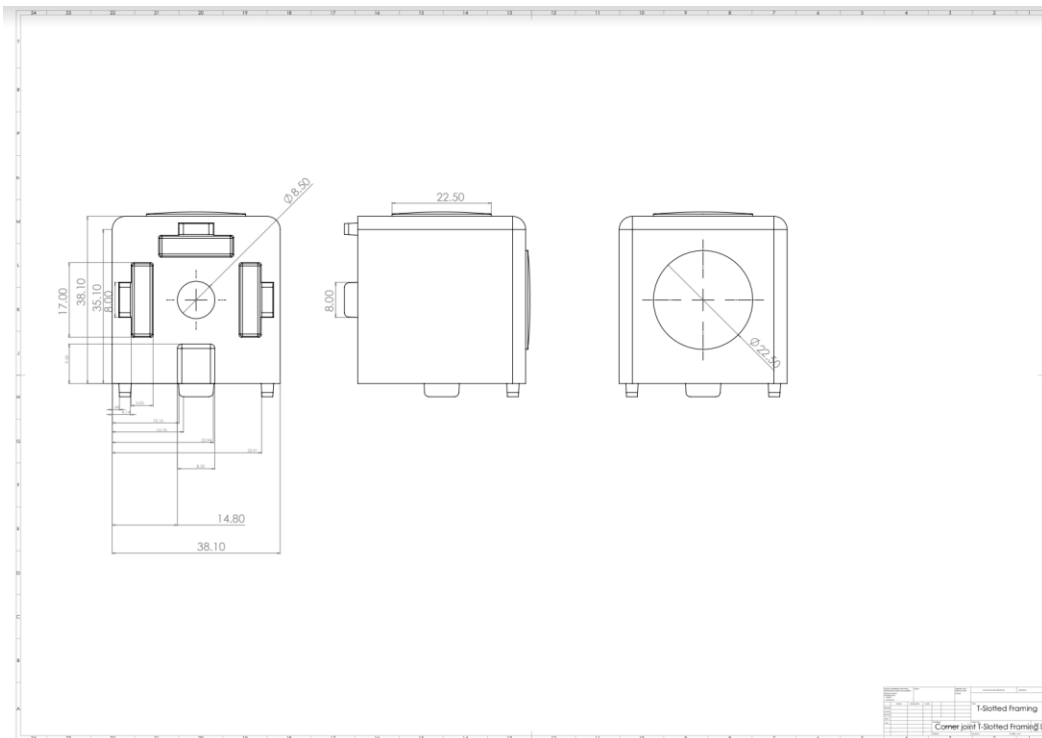
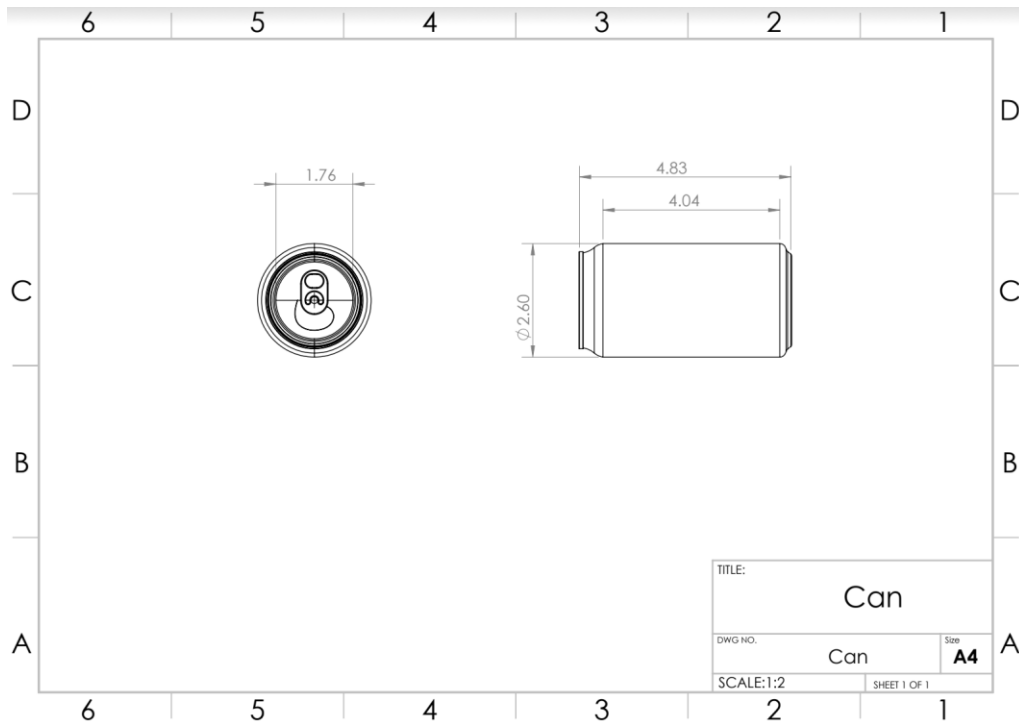
630 Second Street
Portsmouth, Ohio 45662 USA
Voice: 740-876-4936
Email: sales@yostlabs.com

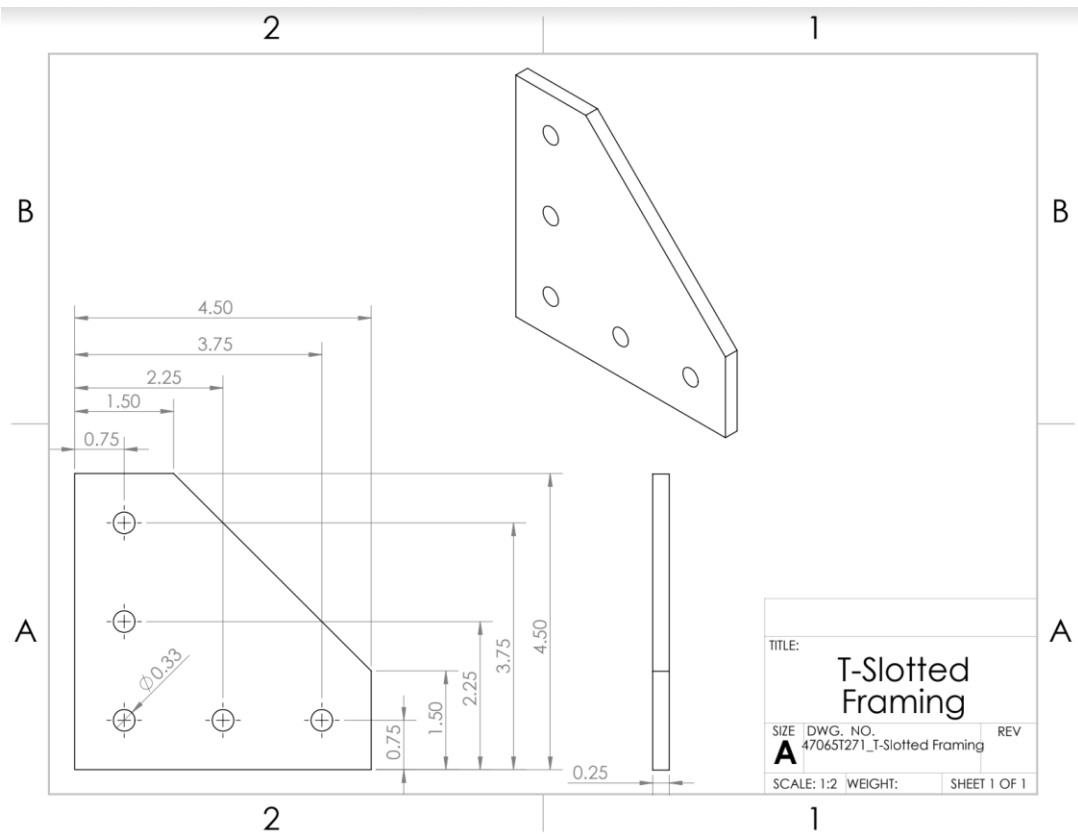
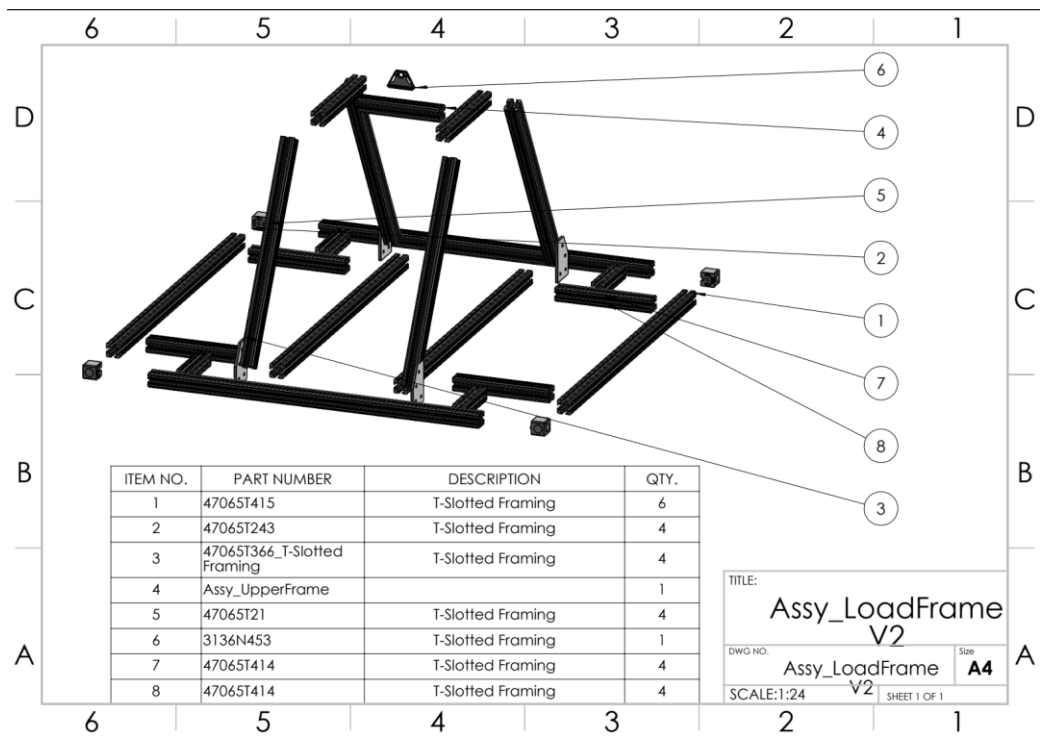
www.YostLabs.com

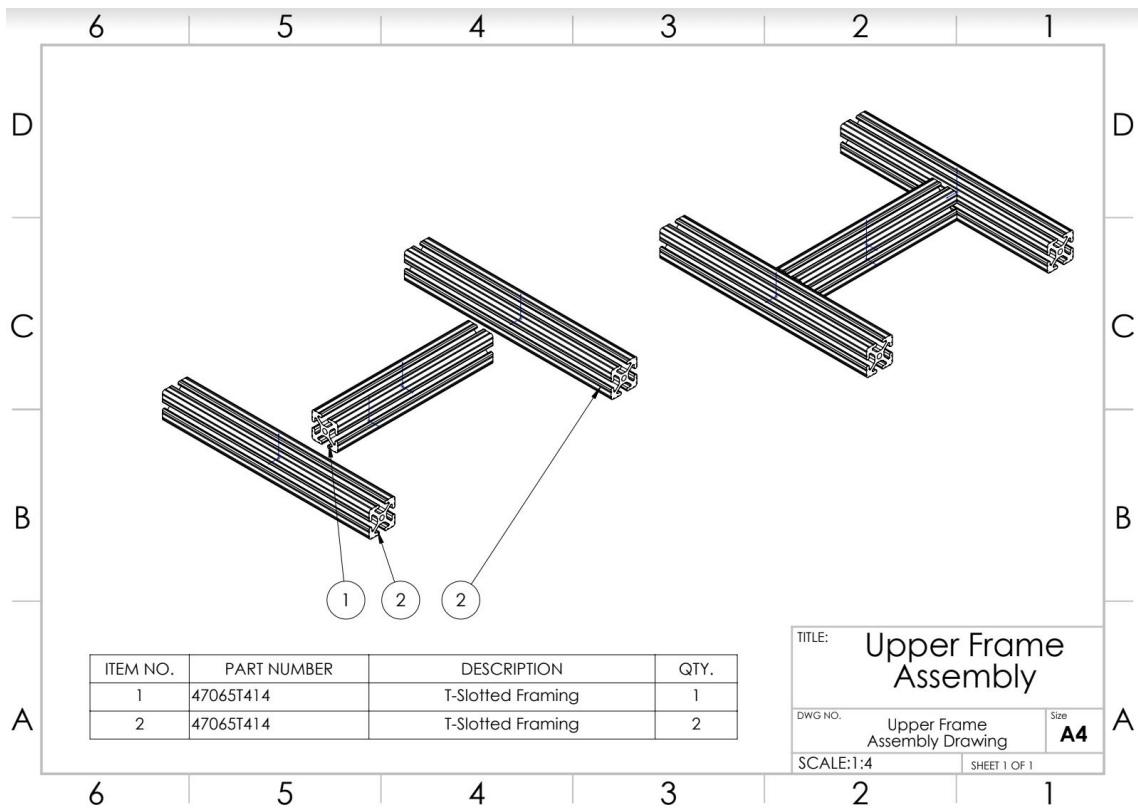
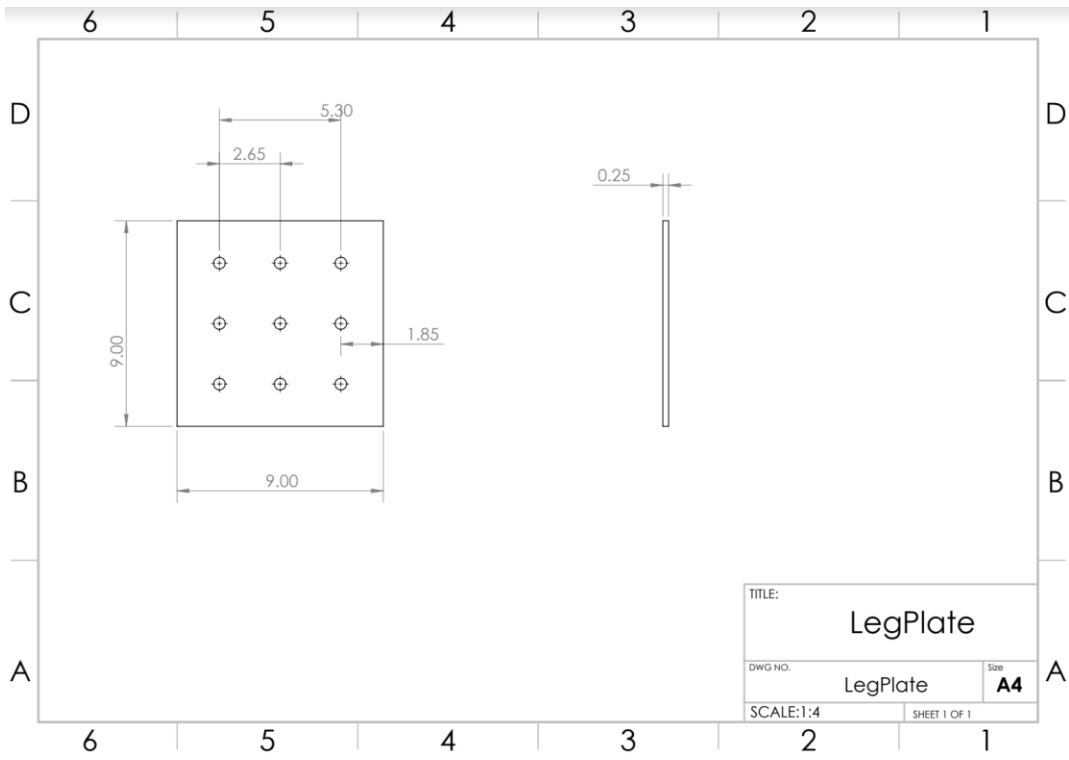
Patents Pending
©2017 Yost Labs, Inc.

Appendix F: Assembly Drawings









Appendix G: Copy of Senior Design Conference Presentation Slide Show

School of Engineering

Mars Rover Crash Vehicle Test Article

Peter Habelt, Gavin Maloney, Ben Rupp, Stan Lieberman, Reid Whitney
Advised by: Drazen Fabris and Nikola Djordjevic

May 12th 2022
Senior Design Conference

www.ecu.edu/engineering

1

School of Engineering

Project Goal

Investigate the feasibility of an economical and readily available impact absorption alternative for Planetary Landing Vehicles.

www.ecu.edu/engineering

2

School of Engineering

Background

Types of Energy Absorption

- Hard Landers
- Semi-Hard Landers
- Shock Absorbers

www.ecu.edu/engineering

3

School of Engineering

Real-World Parameters

NASA'S Opportunity Mars Rover:

- Payload mass of 498 lb
- Total lander mass of 1175 lb
- Impact velocity of 31 mph
- Disipates 52 kJ of energy upon impact

www.ecu.edu/engineering

4

School of Engineering

Past Project

7 years ago, a Senior Design group* demonstrated feasibility of an economical planetary landing vehicle.

This year, we have branched off from that idea by testing a new impact absorption configuration and frame design.

*2015 Project: Proof of Concept Planetary Lander Test Article

www.ecu.edu/engineering

5

School of Engineering

Design Process

- Crumple Zone Subsystem
 - Internal Design
 - Aluminum Cans
 - Aluminum cans serve as crumple zone that will permanently deform, lightweight and cheap, but requires replacing cans after every test.
 - Previously Existing Solution
 - NASA Impact Sphere
 - Incorporates hollow cells that give on impact: cylindrical base and more expensive materials.

www.ecu.edu/engineering

6

School of Engineering

Preliminary Design

www.ecu.edu/engineering

7

School of Engineering

Baseline Testing

- Preliminary testing showed 8 cans would absorb the required 400 J (50 J per can)
- Increased number of cans and retested
- Tested until minimal recoil was observed

www.ecu.edu/engineering

8

School of Engineering

Points of Failure Analysis

- Two points chosen for further analysis
 - Central Beam on Frame
 - will undergo bending during drop testing
 - Corner Bracket
 - will undergo shear stress during drop testing

www.ecu.edu/engineering

9

School of Engineering

Bending Frame Hand Calculations

Given:

- $w = 53.250 \text{ lbs/ft}$
- $L = 36 \text{ in}$
- $I = 0.26 \text{ in}^4$
- $J = 0.75 \text{ in}^4$

Max Bending Stress: 8,629 lbin, 24.9 ksi

www.ecu.edu/engineering

10

School of Engineering

Bending Frame F.E.A.

Max Bending Stress = 15.85 ksi

Compared to hand calculation 24.9ksi

www.ecu.edu/engineering

11

School of Engineering

Corner Mount Analysis

Hand Calculation:

FEA Shear Stress: 24.00 ksi

Factor of Safety: 2.16

FEA Factor of Safety: 2.42

www.ecu.edu/engineering

12

School of Engineering

Design Iterations

- Redesigned crumple zone subsystem as shown
- Increased travel of crumple zone increases energy absorption of the total system during compression
- Splitting crumple zone into 4 legs allows for system to better cope with landing tilt

www.ecu.edu/engineering

13

School of Engineering

Budget

| Item | Amount | Cost per unit (after tax) | Total Cost |
|-----------------------------|--------|---------------------------|------------------|
| Tubular Beam (200 Aluminum) | 200 | \$12.00 | \$2400.00 |
| Frame Brackets | 20 | \$10.00 | \$200.00 |
| Fasteners | 7 | \$4.48 | \$31.36 |
| Aluminum Cans | 144 | \$0.60 | \$86.40 |
| Steel Spring Accelerometer | 1 | \$100.00 | \$100.00 |
| Double F1 Beams | 1 | \$5.00 | \$5.00 |
| Planolet Shims | 6 | \$31.31 | \$187.86 |
| Paint | 1 | \$60.00 | \$60.00 |
| Fasteners | 30 | \$1.48 | \$44.40 |
| Eye Bolt with Nuts | 1 | \$9.37 | \$9.37 |
| TOTAL | | | \$2884.39 |

www.ecu.edu/engineering

14

School of Engineering

Final Configurations

- Crumple columns
- More robust frame to accommodate
- Omission of Shock Assembly

www.ecu.edu/engineering

15

School of Engineering

Safety Protocols for Testing

- Plywood as a partition and ground protection
- Contacted Campus Safety to ensure parking lot was cleared, made warnings visible when testing
- Iron railing was deemed safe for loading when referencing OSHA building codes

www.ecu.edu/engineering

16

School of Engineering

Ground Support Equipment

- 4"x4" Douglas Fir in a cantilever configuration
- Factor of Safety: 3.75 under a 50kg load
- Attached to the railing
- Each cable tie is rated at 136 lb load → 6 cable ties situated every 20" along the vertical outlabeled the 2200 lb moment.
- 6" wood screws
- For higher tensile strength

www.ecu.edu/engineering

17

School of Engineering

Data Acquisition Equipment

- Accelerometer
 - Sampling rate: 250Hz
 - Resolution: 12 bit
 - 2.4GHz Bluetooth
- Recorded linear accelerations
- Slow motion camera
 - Recorded at 184 fps
 - 1080p


www.ecu.edu/engineering

18

SCHOOL OF ENGINEERING
School of Engineering

Drop Test

- Drop Height of 8 feet
- Weight: 70.0 lbs (31.75 kg)
- Guided by pulley; released manually
- 144 cans in a 3x3x4 LWH oriented square to the impact area




www.ecs.uakron.edu/engineering

19

SCHOOL OF ENGINEERING
School of Engineering

Test Results

- = Cans were the only material to show any plastic deformation
 - = Frame, plates, dowels all unharmed
- = Top and bottom layers of cans were deformed the most
- = Acrylic plates and dowels did not break
 - = prove all the energy was absorbed by the crumpled cans



www.ecs.uakron.edu/engineering

20

SCHOOL OF ENGINEERING
School of Engineering

Test Results

- = Energy absorbed by the crumpled cans was 19.81 J (per can)
- = Previously calculated 50 J per can (preliminary testing in fall)
- = After two drop tests...
 - = 72 cans completely crumpled
 - = 64 cans completely unharmed
 - = 3.875" of crumple for each leg (on average)

Energy Absorbed by the Crumpled Cans

$$E_c = mgh = 19.81 \text{ J}$$

$$E_s = \frac{1}{2}mv^2 = 19.81 \text{ J}$$

$$E_t = 50 \text{ J} - 19.81 \text{ J} = 30.19 \text{ J}$$

$$E_c = 72 \times 19.81 \text{ J} = 1426.32 \text{ J}$$

$$E_s = 64 \times 19.81 \text{ J} = 1267.84 \text{ J}$$

$$E_t = 30.19 \text{ J} \times 64 = 1932.16 \text{ J}$$

$$E_c = 1426.32 \text{ J} + 1267.84 \text{ J} + 1932.16 \text{ J} = 4626.32 \text{ J}$$

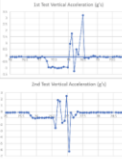
www.ecs.uakron.edu/engineering

21

SCHOOL OF ENGINEERING
School of Engineering

Accelerometer Data

- 2.4GHz Bluetooth
- Sampling rate: 250Hz
- Resolution: 12 bit
- Maximum acceleration recorded ($V_{\text{max}} = 15.66 \text{ mph}$):
 - = Test 1: 3.21 g's
 - = Test 2: 6.58 g's
- NASA Mars Opportunity Rover systems test to rating of 26.4 g's ($V_{\text{max}} = 31 \text{ mph}$)



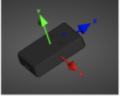
www.ecs.uakron.edu/engineering

22

SCHOOL OF ENGINEERING
School of Engineering

2nd Round Testing Plans

- = Use of three accelerometers
- = Updated accelerometer settings:
 - = 1350 Hz sampling rate
 - = Oversampling
- = Increase sprung mass
 - = Added 22kg of sprung mass to frame
 - = Increases total system mass to 120lbs (54 kg)



www.ecs.uakron.edu/engineering

23

SCHOOL OF ENGINEERING
School of Engineering

Learning Points

- = Testing
 - = Refine the testing method
 - = More tests with different configurations
- = Manufacturing
 - = Dowels needed more clearance
 - = Burns in cans restricted dowel movement
- = Campus Safety restrictions
 - = Higher drops must be conducted off-campus using other methods/procedures

www.ecs.uakron.edu/engineering

24

SCHOOL OF ENGINEERING
School of Engineering

Potential for Future Projects

- = Implementation of shock absorbers
- = Drop from greater height
- = Variety of aluminum can layout, other types of cylinders/materials

www.ecs.uakron.edu/engineering

25

SCHOOL OF ENGINEERING
School of Engineering

Possibility of Implementation

Going back to NASA Mars Opportunity Mission


- = Airbag system dissipated 52 kJ energy on impact
- = Using minimum absorption tested per can (19.81 J), 2625 cans required
- = This would take up 1.4m³ with an added mass of 35.1 kg (~7% of lander mass)



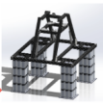
www.ecs.uakron.edu/engineering

26


SCHOOL OF ENGINEERING
School of Engineering



Fall



Winter




Spring

www.ecs.uakron.edu/engineering

27

SCHOOL OF ENGINEERING
School of Engineering

Gantt Charts



www.ecs.uakron.edu/engineering

28